NASA TECHNICAL NOTE

NASA TN D-2386

HEAT TRANSFER ON UNSWEPT AND 38° SWEPT CYLINDRICALLY BLUNTED WEDGE FINS IN FREE FLIGHT TO MACH NUMBER 4.11

by Floyd G. Howard

Langley Research Center
Langley Station, Hampton, Va.

NATIONAL AERONAUTICS AND SPACE ADMINISTRATION • WASHINGTON, D. C. • AUGUST 1964

HEAT TRANSFER ON UNSWEPT AND 38° SWEPT CYLINDRICALLY BLUNTED WEDGE FINS IN FREE FLIGHT TO MACH NUMBER 4.11

By Floyd G. Howard

Langley Research Center
Langley Station, Hampton, Va.

NATIONAL AERONAUTICS AND SPACE ADMINISTRATION

For sale by the Office of Technical Services, Department of Commerce,
Washington, D.C. 20230 -- Price $1.25

HEAT TRANSFER ON UNSWEPT AND 38° SWEPT CYLINDRICALLY BLUNTED WEDGE FINS IN FREE FLIGHT TO MACH NUMBER 4.11

By Floyd G. Howard
Langley Research Center

SUMMARY

Heat-transfer measurements were obtained on the cylindrically blunted leading edge and along the midspan chord of unswept and of 38° swept wedge-section fins in free flight for a Mach number range from 1.70 to 4.11. Free-stream Reynolds numbers per foot varied from 8.2×10^6 to 16.5×10^6. Comparison of theoretical and experimental heat-transfer results indicates that the boundary layer over the cylindrically blunted leading edge of the unswept fin was laminar throughout the test. On the 38° swept fin, the boundary layer was turbulent at free-stream Reynolds numbers (based on leading-edge diameter) as low as 0.362×10^6 and appears to have been turbulent throughout the test with Reynolds numbers as low as 0.256×10^6. On the leading edge, the laminar and the turbulent heat transfer at the stagnation line of the unswept and the swept fin, respectively, were in good agreement with theories for a yawed cylinder. On the unswept leading edge 45° from the stagnation line, the laminar theories were in fair agreement with data. On the 38° swept leading edge 45° from the stagnation line and at the tangency point of both leading edges, the data were considerably higher than the theories. The laminar and turbulent heating on the wedge surfaces were in fair agreement with flat-plate theory. Local transition Reynolds numbers on the wedge surface of the unswept fin varied between 0.65×10^6 and 4.63×10^6 with transition reversal occurring when the ratio of wall temperature to local stream temperature was lowest.

INTRODUCTION

Supersonic heat transfer to cylindrical leading edges of bodies has been investigated in several wind-tunnel programs (for instance, refs. 1 and 2) and some free-flight programs (refs. 3 and 4), and theoretical analyses have been developed for both the swept and unswept case (ref. 1). Although it has been generally considered advantageous to sweep the leading edge of fins or wings in order to reduce the drag and leading-edge heating, theory and data (ref. 1) indicate the reduction in heating expected by sweeping the leading edge may be more than canceled by the occurrence of turbulent flow along the stagnation line of the swept wing with blunt leading edge.

To study the effects of sweep further, an investigation of heat transfer on the cylindrical leading edge and along the midspan chord of an unswept and a 38° swept fin was conducted and the results are presented herein. This flight test was conducted at Wallops Island, Va. as part of a general flight program to study the effects of fin geometry on supersonic heat transfer to fins or wings. Data were obtained from Mach numbers 1.70 to 4.11 over a Reynolds number range from 8.2×10^6 to 16.5×10^6 per foot.

SYMBOLS

b	surface distance measured from stagnation line in plane perpendicular to leading edge and used only on cylindrical surface of fin (eq. (10)), in.
c_p	specific heat at constant pressure, Btu/lb-°R
D	leading-edge diameter, in.
h	heat-transfer coefficient, Btu/ft^2-sec-°R
k	thermal conductivity, $\frac{\text{Btu-ft}}{\text{ft}^2\text{-sec-}^\circ\text{R}}$
M	Mach number
p	pressure, lb/ft^2
N_{Pr}	Prandtl number
q	heat-transfer rate, Btu/ft^2-sec
R	Reynolds number
r	outside radius, in.
s	surface distance measured from stagnation line of fin in stream direction (fig. 2), in.
T	temperature, °R
t	time, sec
x	chordwise distance measured from stagnation line of fin (fig. 2), in.
y	spanwise distance measured from root of fin, in.
γ	ratio of specific heats

ϵ	emissivity
η	recovery factor
θ	azimuth angle, deg
Λ	sweep angle, deg
ρ	density, slugs/ft^3
ρ'	specific weight for inconel, 518.4 lb/ft^3
σ	Stefan-Boltzmann constant, 4.835×10^{-13}, Btu/ft^2-sec($^\circ$R)^4
τ	skin thickness, in.

Subscripts:

aero	aerodynamic
aw	adiabatic wall conditions
c	conduction
D	based on leading-edge diameter
eff	effective
iw	inside wall
L	laminar
l	based on local conditions
m	measured
ow	outside wall computed by use of reference 1
r	radiation
s	conditions at stagnation line
t	total
tr	transition
w	wall
∞	free-stream conditions

TEST VEHICLE AND FINS

The data of this investigation were obtained from measurements on stabilizing fins mounted symmetrically on a Cajun motor. As shown in figures 1 and 2, two of the four-wedge stabilizing fins were unswept and two were swept 38°. One of each type was instrumented with thermocouples. A 10° wedge section was used for the fins because of its relatively high stabilizing effectiveness at the high Mach numbers of the flight test.

The fins were constructed from 0.05-inch inconel sheeting with internal ribs and spars. Aft of $x = 1$ inch measured in stream direction from the stagnation line, the skin was chemically milled to a thickness of approximately 0.035 inch. Locations of the ribs and spars within the fins were such (at least 1.3 inches from nearest thermocouple) that they would not serve as heat sinks at the location of heat-transfer measurements which were made on the leading edge and along the semispan chord of each fin. Location of heat-transfer measurements and pertinent details of test fins are shown in figure 2.

A blunted ogive nose mounted on the Cajun motor carried the telemeter, four accelerometers, and two spike antennas arranged so that the fins were not directly in the wake. Details of the general configuration are shown in figure 1(b).

INSTRUMENTATION

Skin temperatures were measured during the flight by means of 24 thermocouples made of number 30 gage chromel-alumel wires and spotwelded on the inside surface of the skin. Thermocouples were located to provide measurements along the stagnation line, at a θ of 45°, at a tangency point, and at several points along the midspan chord of both the swept and unswept fins. (See fig. 2.) These data were transmitted through 2 channels of telemetry with each channel accommodating 12 thermocouples and 3 reference voltages. The commutation rate was such that the temperature at each thermocouple location was recorded every 0.2 second. The reference voltages, also recorded every 0.2 second, were selected equivalent to the lowest temperature, the midrange temperature, and the highest temperature that the skin thermocouples were expected to reach, and thus supplied an in-flight check for calibration of the temperature measurement system. Other information telemetered during the test included continuous measurements of normal, transverse, thrust, and drag accelerations.

TRAJECTORY DATA

The three-stage vehicle used in this investigation is shown on the launcher in figure 3 at the elevated launch angle of 70°. The first-stage Nike motor boosted the test vehicle to a Mach number of 1.44. After a 9-second coast period the second-stage Nike boosted the test vehicle to a Mach number of 4.11. After a 19-second coast period the Cajun motor ignited and boosted the test vehicle to a Mach number of 6.30. All three stages burned during the ascending

portion of the trajectory. However, no telemeter signal was received between 22 seconds and 43 seconds of flight time which includes the entire third-stage heating period; therefore, no heat-transfer data are shown after 20 seconds. Up to the time the telemeter transmission stopped the normal and transverse acceleration data indicated no appreciable angle of attack during the test.

Trajectory data for the test vehicle were obtained from NASA modified SCR-584 and AN/FPS-16 position radar. In addition, velocity during the early portion of the flight was supplied by CW Doppler radar. Time histories of velocity and altitude are shown in figure 4(a). Mach number and Reynolds number per foot (fig. 4(b)) were computed by using free-stream density, pressure, and temperature as determined from radiosondes launched near flight time and tracked by rawinsonde. These ambient atmospheric conditions correlated with flight time are shown in figure 5.

EXPERIMENTAL HEAT TRANSFER

Data Reduction

The faired inside surface temperature curves for each measurement location are presented in figure 6. As shown in this figure the highest heating rates occurred between 13 seconds and 20 seconds (which covered a Mach number range from 1.70 to 4.11); therefore, data are analyzed only for this period.

Shown in figure 7 are the temperature-time data for thermocouple 15, which are typical of commutation frequency and experimental scatter. Similar faired inside surface temperature curves were used in conjunction with Hill's method of reference 5 to compute outside surface temperature histories as indicated in figure 7. For those thermocouples located on the aft portion of the fins where the computations indicated a very small temperature gradient through the wall, the outside temperature was assumed to be equal to the inside temperature.

The experimental heat-transfer rates uncorrected for conduction and radiation are equal to the rate of heat storage within the skin as expressed by the equation

$$q_m = \rho' \frac{\tau_{eff}}{\tau_m} \frac{1}{12} \int_0^{\tau_m} \left(c_p \frac{dT}{dt} \right) d\tau \tag{1}$$

To evaluate q_m it was assumed that

$$\rho' \frac{\tau_{eff}}{\tau_m} \frac{1}{12} \int_0^{\tau_m} \left(c_p \frac{dT}{dt} \right) d\tau = \rho' \frac{\tau_{eff}}{24} \left(c_p \frac{dT_{iw}}{dt} + c_p \frac{dT_{ow}}{dt} \right) \tag{2}$$

Values of dT/dt were obtained by mechanically differentiating the faired temperature time history curves, and the specific heat c_p of inconel was obtained as a function of temperature from reference 6. The effective skin

thickness at locations on the leading edge is somewhat less than the actual skin thickness because of the curvature of the leading edge; therefore, the effective thickness was obtained by dividing the volume of a cylindrical segment by the surface area of the segment as shown by the following expression:

$$\tau_{eff} = \frac{\pi\left[r^2 - (r - \tau_m)^2\right] \times \frac{\Delta\theta}{360} \times \text{Unit length}}{2\pi r \times \frac{\Delta\theta}{360} \times \text{Unit length}} \tag{3}$$

$$\frac{\tau_{eff}}{\tau_m} = 1 - \frac{\tau_m}{2r} \tag{4}$$

which yields $\tau_{eff} = \tau_m(0.864)$ for cylindrical portions of the fins of this investigation. At the point of tangency, a value of $\frac{1}{2}(1 + 0.864) = 0.932$ was used to obtain the effective skin thickness.

The heat-transfer rates for thermocouple 15 were also computed by use of Hill's method (ref. 5) and the two methods produced almost identical heating rates for thermocouple 15.

Conduction and Radiation Corrections

In figure 8 spanwise distributions of stagnation-line temperatures are shown for both the swept and unswept fins. With the assumption of linear temperature distribution between measurement points, spanwise conduction was computed and was found to be negligible.

Figures 9(a) and 9(b) show chordwise temperature distributions along the instrumented chord on the unswept and swept fin, respectively. Computations based on these distributions showed that the effect of chordwise conduction at measurement locations on wedge section of the fins was only 1 Btu/ft^2-sec or less even at the most forward thermocouple locations (thermocouples 7 and 20) where the highest thermal gradients occurred. Chordwise conduction was therefore neglected for the measurement stations on the wedge section of the fins. Chordwise conduction could not be neglected, however, at the stagnation line, at $\theta = 45^\circ$, and at the tangency points of the leading edges. Chordwise conduction corrections for these measurement locations were computed in the following manner. The temperatures at closer intervals than the measurements provided were determined by use of the theoretical stagnation-line heat-transfer and theoretical heat-transfer distribution in conjunction with a computer program. These temperatures were used to compute the conduction at the stagnation line, at $\theta = 45^\circ$, and at the tangency point by use of the following sketch and expression.

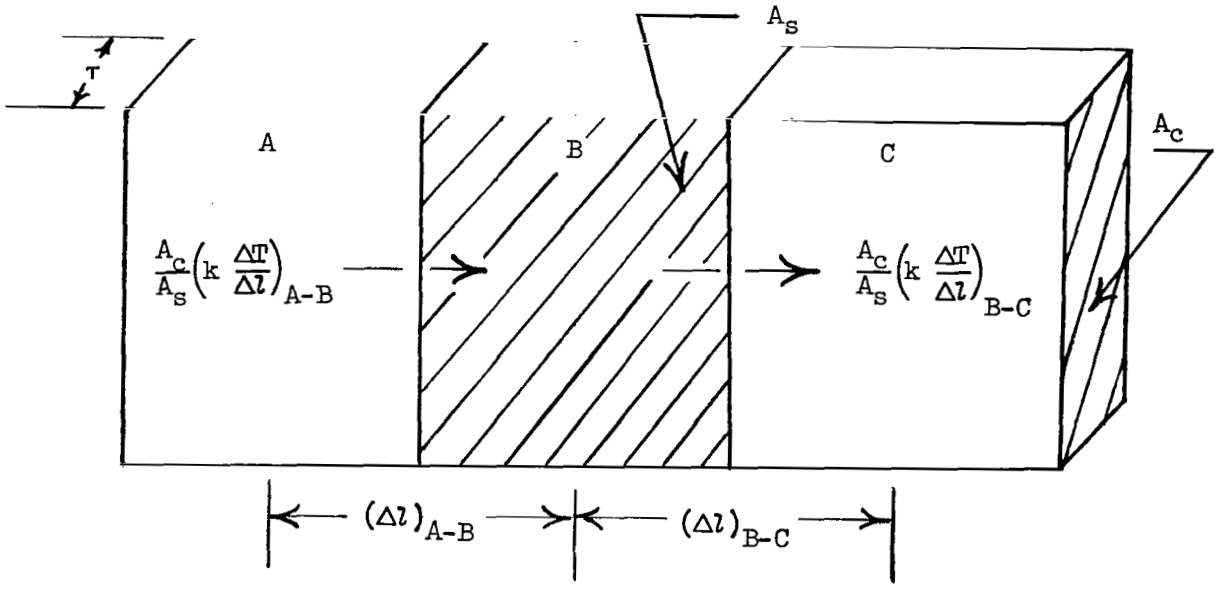

$$(q_c)_B = \frac{A_c}{A_s}\left[\left(k\frac{\Delta T}{\Delta l}\right)_{A-B} - \left(k\frac{\Delta T}{\Delta l}\right)_{B-C}\right] \tag{5}$$

where A_c is the conductive area, A_s is the surface or convective area, and l is distance.

The heat loss due to radiation was negligible at locations on the wedge section, but was computed for measurement locations on the leading edge by use of a constant emissivity ϵ of 0.65 in the following equation:

$$q_r = \epsilon\sigma T_{ow}^{4} \tag{6}$$

where T_{ow} is in degrees Rankine. Corrections for conduction and radiation at the stagnation line are shown in figure 10.

The experimental aerodynamic heating rates were obtained by adding the corrections for conduction and for radiation to the measured heating rates as shown in the following equation:

$$q_{aero} = q_m + (q_c + q_r) \tag{7}$$

THEORETICAL HEAT TRANSFER

Since the angular orientation of the antennas with respect to the fin was such that wake effects were minimized and computations showed that the maximum body boundary-layer thickness was 2.25 inches or less (refs. 7 and 8),

disturbances on the fins due to these effects were considered to be negligible. Therefore, the conditions ahead of the fin shock were assumed to be free-stream conditions.

Theoretical heating rates for the flight conditions were computed for comparison with the experimental results by use of the basic expressions

$$q = h\left(T_{aw} - T_{ow}\right) \tag{8}$$

$$T_{aw} = \eta\left(T_t - T_l\right) + T_l \tag{9}$$

where T_{ow} is the outside wall temperature (for example, dashed line in fig. 7) and T_{aw} is the adiabatic wall temperature computed from the flight conditions and theoretical recovery factor. Recovery factors, $N_{Pr}^{1/2}$ for laminar flow and $N_{Pr}^{1/3}$ for turbulent flow, were evaluated at the outside wall temperature T_{ow}.

Theoretical stagnation-line heat-transfer coefficients for the swept and unswept leading edges were evaluated from the theories of reference 1. For locations on the cylindrical leading edge other than the stagnation line, the theoretical laminar distributions h/h_s of both reference 1 and reference 2 were used for the unswept fin. The theoretical turbulent distribution h/h_s of reference 1 was used for the swept fin.

On the wedge section, heat-transfer coefficients were determined by use of Van Driest's flat-plate theory (ref. 9) evaluated at local conditions.

The local conditions were computed by use of the ideal-gas relations of reference 10. Static pressure and total pressure on the unswept stagnation line are equivalent and equal to the total pressure behind the normal shock. Static pressure along the stagnation line on the swept leading edge was computed by using the Mach number normal to the leading edge in the Rayleigh pitot formula of reference 10.

The static-pressure distribution around the cylindrical leading edges as a function of stagnation-line pressure was obtained from the following empirical equation of reference 2

$$\frac{p_l}{p_s} = \left[1 - \frac{\gamma - 1}{2}\left(2.13\,\frac{b}{D}\right)^2\right]^{\frac{\gamma}{\gamma-1}} \tag{10}$$

The static pressure on the wedge sections was taken as the two-dimensional wedge pressure from reference 10. Local total pressure was assumed to be equal to the total pressure behind the shock lying along the leading edge (that is, shock angle equal to $90^\circ - \Lambda$).

RESULTS AND DISCUSSION

Leading Edge

The experimental stagnation-line heating rates measured at the midspan locations of the unswept and swept fin are shown in figure 11. Theoretical laminar and turbulent heating rates, evaluated by the method of reference 1, are plotted for comparison. The measured (that is, uncorrected) heating rates are considerably less than the theoretical rates, but when corrected for the heat flow away from the stagnation line due to conduction and radiation, the measurements are in good agreement with the laminar theory for the unswept leading edge and with the turbulent theory for the swept leading edge. Under the particular conditions of this test turbulent heating at the stagnation line of the 38° swept fin was about 20 percent greater than the laminar heating on the unswept fin, and conduction and radiation on each fin had the effect of reducing stagnation-line heating by about 20 percent.

Figure 12 shows the corrected experimental heating rates for all stagnation-line measurement stations. On each fin the same corrections for conduction and radiation were used at all spanwise stations since there were only slight variations in stagnation-line temperatures.

Theoretical heat-transfer rates were slightly different for each thermocouple location on each fin because of their slightly different temperature time histories. The theoretical curve shown for each sweep angle is the average of the maximum and the minimum theoretical values. In general, the computed theoretical values for the individual locations differed from the average theoretical curve by less than ± 3 Btu/ft^2-sec except at about 16 seconds where the difference was less than ± 6 Btu/ft^2-sec.

On the unswept leading edge, good agreement is shown in the experimental results for the four spanwise locations and between the experimental results and laminar theory. No spanwise variations are apparent. Data from the stagnation line of the 38° swept fin are in good agreement with the turbulent theory although there is some experimental scatter.

A comparison of the heat-transfer coefficients h at the stagnation line on the swept and the unswept fin is shown in figure 13. The experimental heat-transfer coefficients were obtained from the experimental heating rates as follows:

$$h_{aero} = \frac{q_{aero}}{T_{aw} - T_{ow}} \tag{11}$$

Near the times of zero heat transfer (that is, when $T_{aw} = T_{ow}$) the experimental values of h tend to scatter and diverge because both the numerator and denominator of equation (11) approach zero simultaneously, thus the effects of errors in either are magnified. Therefore, all points in that region are not shown. Based on the comparison with theory of reference 1 (fig. 13), the heat-transfer coefficient data indicate laminar flow on the unswept stagnation line and turbulent flow on the swept stagnation line as was also indicated by the

heating-rate data of figure 12. It may be noted that the maximum values of h were approximately twice as high on the stagnation line of the 38° swept fin with turbulent flow as on the unswept fin with laminar flow, even though the corresponding heating rates q were only about 20 percent higher at the particular conditions of this test.

Shown in figure 14 are the experimental heating-rate data in comparison with theory for locations at $\theta = 45^\circ$ and at the tangency point. The predictions at $\theta = 45^\circ$ were in reasonably good agreement with data for the unswept fin and slightly low for the swept fin. The theoretical laminar predictions at the tangency point of the unswept fin were slightly lower than values obtained from experimental data, but the turbulent predictions were less than half the experimental values obtained for the swept fin.

Experimental and theoretical distributions of heating rates around the unswept and swept leading edges are shown in figure 15. It is apparent that the overall heating is much greater on the swept fin.

Wedge Section

A comparison of experimental heat transfer with theoretical heat transfer for the wedge section of the unswept fin is shown in figure 16. The flow at the most forward location (thermocouple 7, fig. 16(a)) was laminar during the entire heating period, although the experimental data are slightly higher than the laminar theory of reference 9. Both laminar and turbulent heating rates occurred at thermocouples 8, 9, and 10 (figs. 16(b), 16(c), and 16(d)) at different times during the test. The two rearmost locations, thermocouples 11 and 12 (figs. 16(e) and 16(f)) had turbulent heating rates throughout the test. There is fair agreement between the data and the turbulent flat-plate theory of reference 9, the local Reynolds number being based on surface distance from the stagnation line.

The flow at all thermocouple locations on the swept fin is turbulent during the entire heating period. As shown in figure 17 the turbulent flat-plate theory of reference 9 based on surface distance from the stagnation line agrees fairly well with the experimental data.

Transition

Unswept fin.- The heat-transfer data shown in figure 16 indicate that during the test the location of boundary-layer transition moved along the wedge section of the unswept fin. The limits of local transition were considered to have occurred between the rearmost station having definitely laminar heating and the next rearward station, even though the latter station may not have had fully turbulent heating. These limits of transition Reynolds number R_{tr} based on surface distance from stagnation line are plotted against the local Mach number M_l, the local Reynolds number R_l per foot, and the temperature ratio T_{ow}/T_l in figures 18(a), 18(b), and 18(c), respectively. (At each time both M_l and R_l per foot have the same value at the two transition-bracketing

stations, but the values of the ratio T_{ow}/T_l are somewhat different.) Curves of R_{tr} which are consistent with time on all three plots were faired between the limits in figure 18.

Although R_{tr} which varied between 0.65×10^6 and 4.63×10^6 is plotted against the individual parameters M_l, R_l per foot, and T_{ow}/T_l, its trends are caused by the simultaneous variations of all three parameters, and, in general, the effects of the individual parameters cannot be isolated. However, during the time period 15.6 to 16.8 seconds (solid symbols in fig. 18), only T_{ow}/T_l changes appreciably; M_l was essentially constant near 2.04 and R_l per foot varied only over the range from 7.70×10^6 to 6.75×10^6. (The expected effect of this small decrease in R_l per foot would be a small decrease in R_{tr} as is shown by wind-tunnel investigations. See, for instance, ref. 11.) Over this time period, R_{tr} doubled as T_{ow}/T_l increased from 0.73 to 1.06. The early transition at the lower temperature ratios indicates the presence of transition reversal. In wind-tunnel investigations of transition on bodies of revolution at test conditions near those of the present test, transition reversal (that is, early transition at cold-wall conditions) has occurred in some instances, but not in others. (See, for instance, ref. 12.) Its occurrence has not been noted in previously reported free-flight data.

Swept fin.- The data of figures 11 and 12 show clearly that the boundary layer on the stagnation line of the swept fin was turbulent between times of approximately 14.4 seconds and 16.8 seconds during which times $R_{D,\infty}$ was as low as 362,000.

The heating rates appear to have been turbulent throughout the test, with $R_{D,\infty}$ as low as 256,000, but before 14.4 seconds and after 16.8 seconds the heating rates are low and the type of flow cannot be identified with complete assurance.

SUMMARY OF RESULTS

Heat-transfer measurements have been obtained on the cylindrically blunted leading edge and along the midspan chord of an unswept and of a 38° swept wedge-section fin in free flight for a Mach number range from 1.70 to 4.11. Free-stream Reynolds number per foot varied from 8.2×10^6 to 16.5×10^6. Results of the investigation are as follows:

1. The boundary layer over the cylindrically blunted leading edge of the unswept fin was laminar throughout the test. On the 38° swept fin, the boundary layer was clearly turbulent at free-stream Reynolds numbers based on leading-edge diameter as low as 0.362×10^6 and appeared to have been turbulent throughout the test with Reynolds numbers as low as 0.256×10^6.

2. On the leading edge, the laminar and the turbulent heat transfer at the stagnation line of the unswept and swept fin, respectively, were in good agreement with theory for a yawed cylinder.

3. On the unswept leading edge, 45° from the stagnation line, the laminar theories (NASA TR R-104 and NACA RM A55H31) were in fair agreement with the experimental heat-transfer data; however, on the 38° swept leading edge 45° from the stagnation line and at the tangency point of both leading edges, the experimental heat-transfer rates were considerably higher than the theories.

4. The laminar and turbulent heating on the wedge surfaces were in fair agreement with flat-plate theory of Van Driest (Aero, Eng. Rev. 1956) evaluated at local conditions.

5. Local transition Reynolds number on the wedge surface of the unswept fin varied between 0.65×10^{6} and 4.63×10^{6} with transition reversal occurring when the ratio of wall temperature to local stream temperature was lowest.

Langley Research Center,
National Aeronautics and Space Administration,
Langley Station, Hampton, Va., April 30, 1964.

REFERENCES

1. Beckwith, Ivan E., and Gallagher, James J.: Local Heat Transfer and Recovery Temperatures on a Yawed Cylinder at a Mach Number of 4.15 and High Reynolds Numbers. NASA TR R-104, 1961. (Supersedes NASA MEMO 2-27-59L.)

2. Goodwin, Glen, Creager, Marcus O., and Winkler, Ernest L.: Investigation of Local Heat-Transfer and Pressure Drag Characteristics of a Yawed Circular Cylinder at Supersonic Speeds. NACA RM A55H31, 1956.

3. O'Neal, Robert L., and Bond, Aleck C.: Heat Transfer to 0° and 75° Swept Blunt Leading Edges in Free Flight at Mach Numbers From 1.90 to 3.07. NASA TN D-1256, 1962.

4. Swanson, Andrew G., and Rumsey, Charles B.: Aerodynamic Heating of a Wing As Determined From a Free-Flight Rocket-Model Test to Mach Number 3.64. NACA RM L56F11a, 1956.

5. Hill, P. R.: A Method of Computing the Transient Temperature of Thick Walls From Arbitrary Variation of Adiabatic-Wall Temperature and Heat-Transfer Coefficient. NACA Rep. 1372, 1958. (Supersedes NACA TN 4105.)

6. Rumsey, Charles B., and Lee, Dorothy B.: Measurements of Aerodynamic Heat Transfer on a 15° Cone-Cylinder-Flare Configuration in Free Flight at Mach Numbers up to 4.7. NASA TN D-824, 1961. (Supersedes NACA RM L57J10.)

7. Schlichting, Hermann (J. Kestin, trans.): Boundary Layer Theory. Fourth ed., McGraw-Hill Book Co., Inc., 1960.

8. Shapiro, Ascher H.: The Dynamics and Thermodynamics of Compressible Fluid Flow. Vol. II. The Ronald Press Co., c.1954.

9. Van Driest, E. R.: The Problem of Aerodynamic Heating. Aero. Eng. Rev., vol. 15, no. 10, Oct. 1956, pp. 26-41.

10. Ames Research Staff: Equations, Tables, and Charts for Compressible Flow. NACA Rep. 1135, 1953. (Supersedes NACA TN 1428.)

11. Potter, J. Leith, and Whitfield, Jack D.: Effects of Unit Reynolds Number, Nose Bluntness, and Roughness on Boundary Layer Transition. Rep. 256, AGARD, North Atlantic Treaty Organization (Paris), Apr. 1960.

12. Jack, John R., and Wisniewski, Richard J.: The Effect of Extreme Cooling and Local Conditions on Boundary-Layer Transition. Jour. Aero/Space Sci. (Readers' Forum), vol. 25, no. 9, Sept. 1958, pp. 592-593.

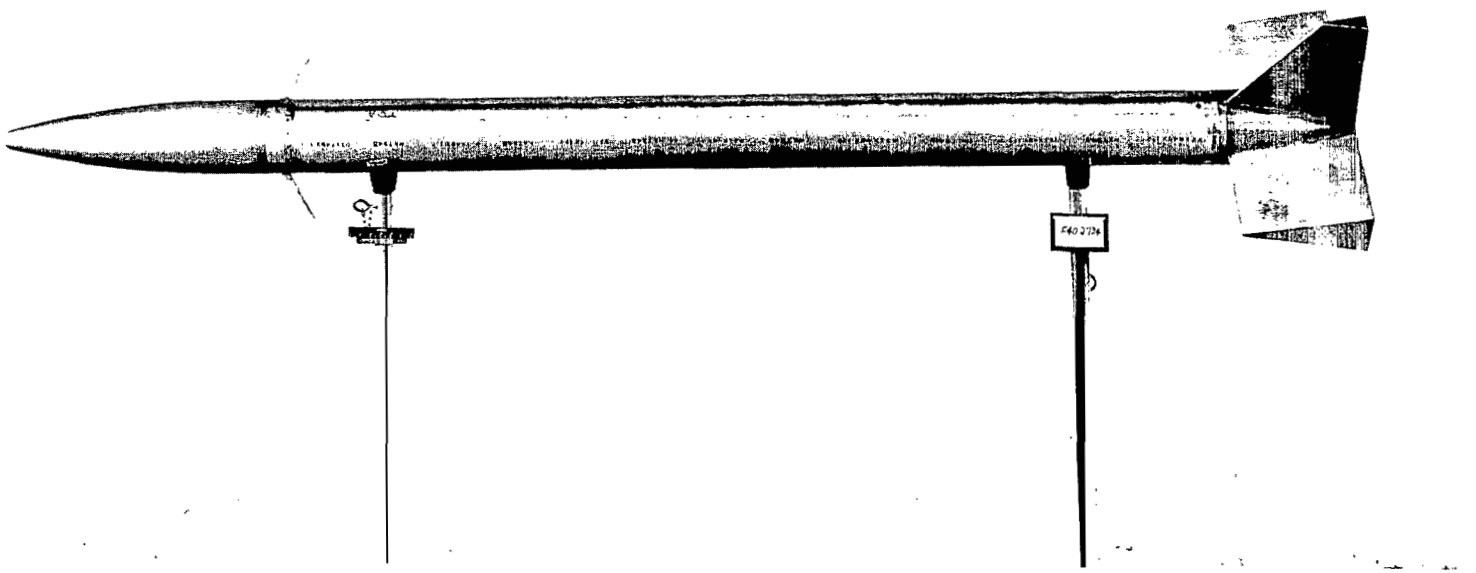

(a) Photograph of test vehicle. L-59-2686

Figure 1.- Test vehicle.

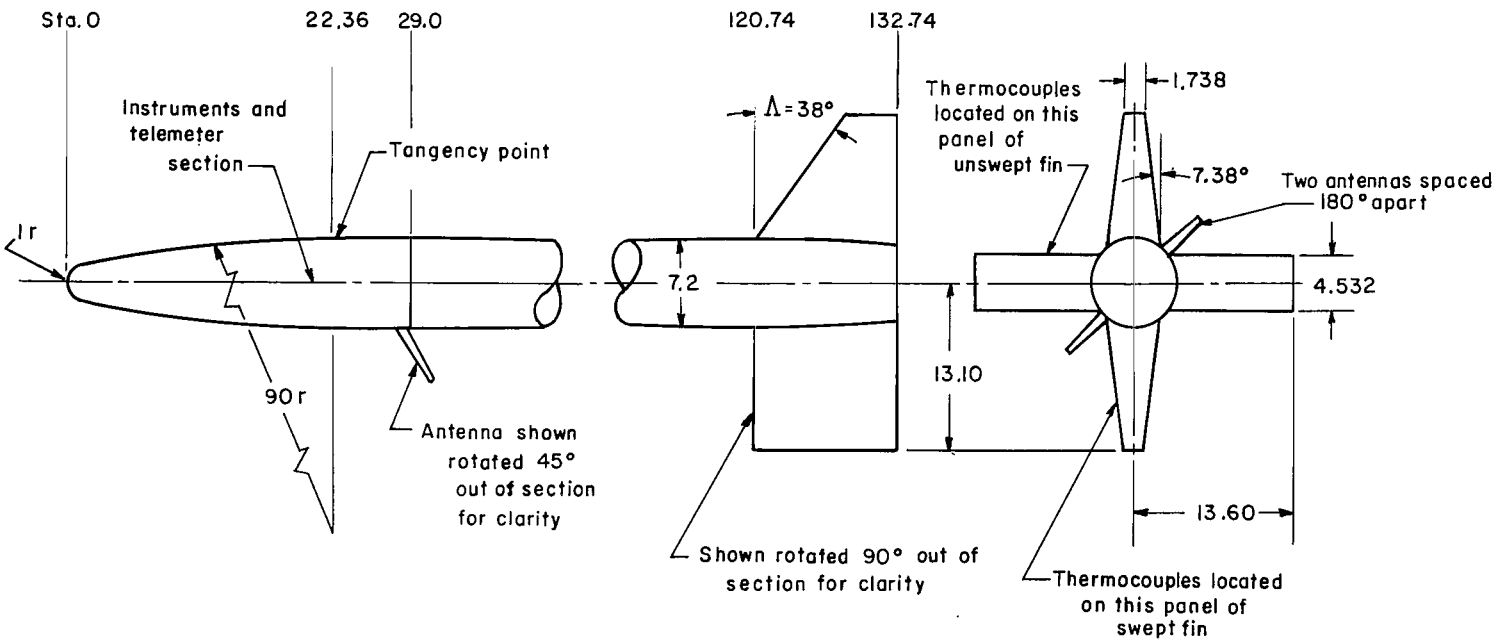

(b) Details of test vehicle. Dimensions are in inches unless otherwise noted.

Figure 1.- Concluded.

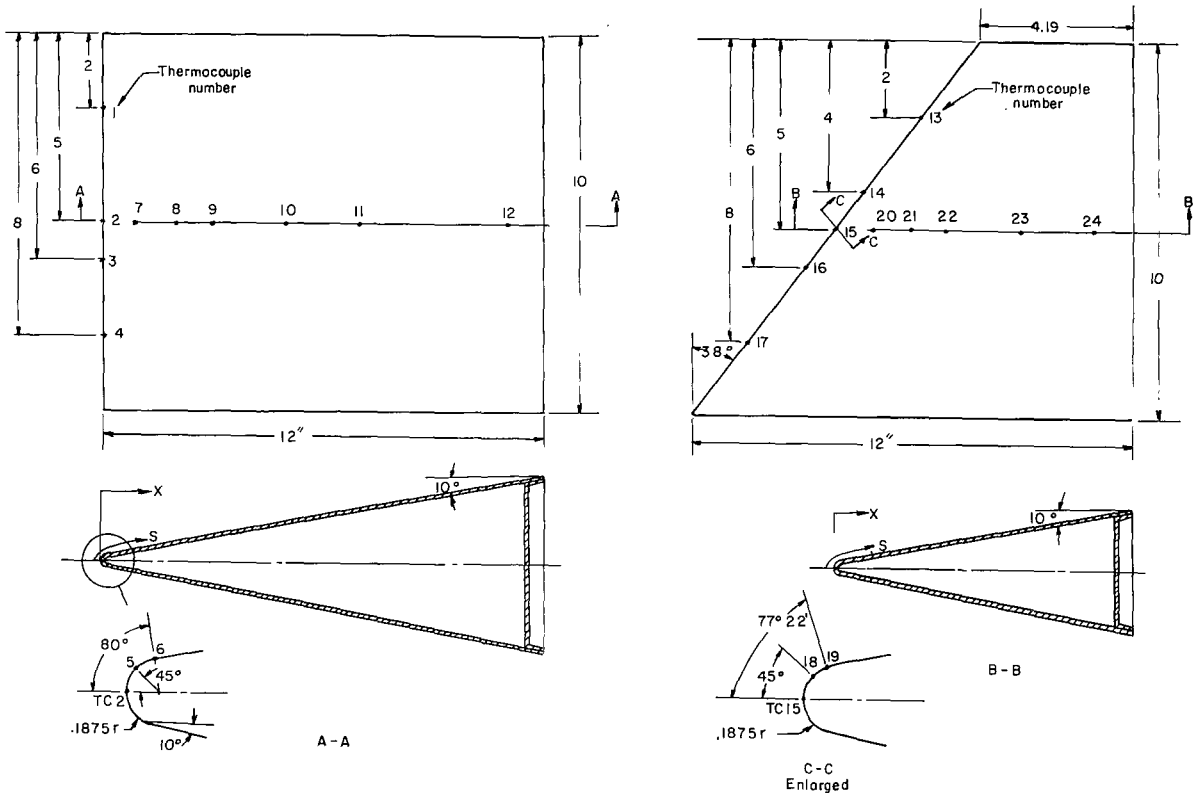

TC	x, in.	s, in.	τ, in.
1	0	0	.0449 *
2	0	0	.0449 *
3	0	0	.0449 *
4	0	0	.0449 *
5	.055	.147	.0449 *
6	.155	.262	.0484 *
7	.9	1.018	.052
8	2.0	2.135	.037
9	3.0	3.151	.037
10	5	5.182	.036
11	7	7.212	.0365
12	11	11.274	.036
13	0	0	.0432 *
14	0	0	.0432 *
15	0	0	.0432 *
16	0	0	.0432 *
17	0	0	.0432 *
18	.070	.156	.0432 *
19	.186	.285	.0466 *
20	.9	1.010	.05
21	2.0	2.127	.032
22	3.0	3.142	.032
23	5	4.607	.036
24	7	7.204	.037

* Effective skin thickness (See eq. 3)

Figure 2.- Details of test fins and locations of thermocouples. Dimensions are in inches unless otherwise noted.

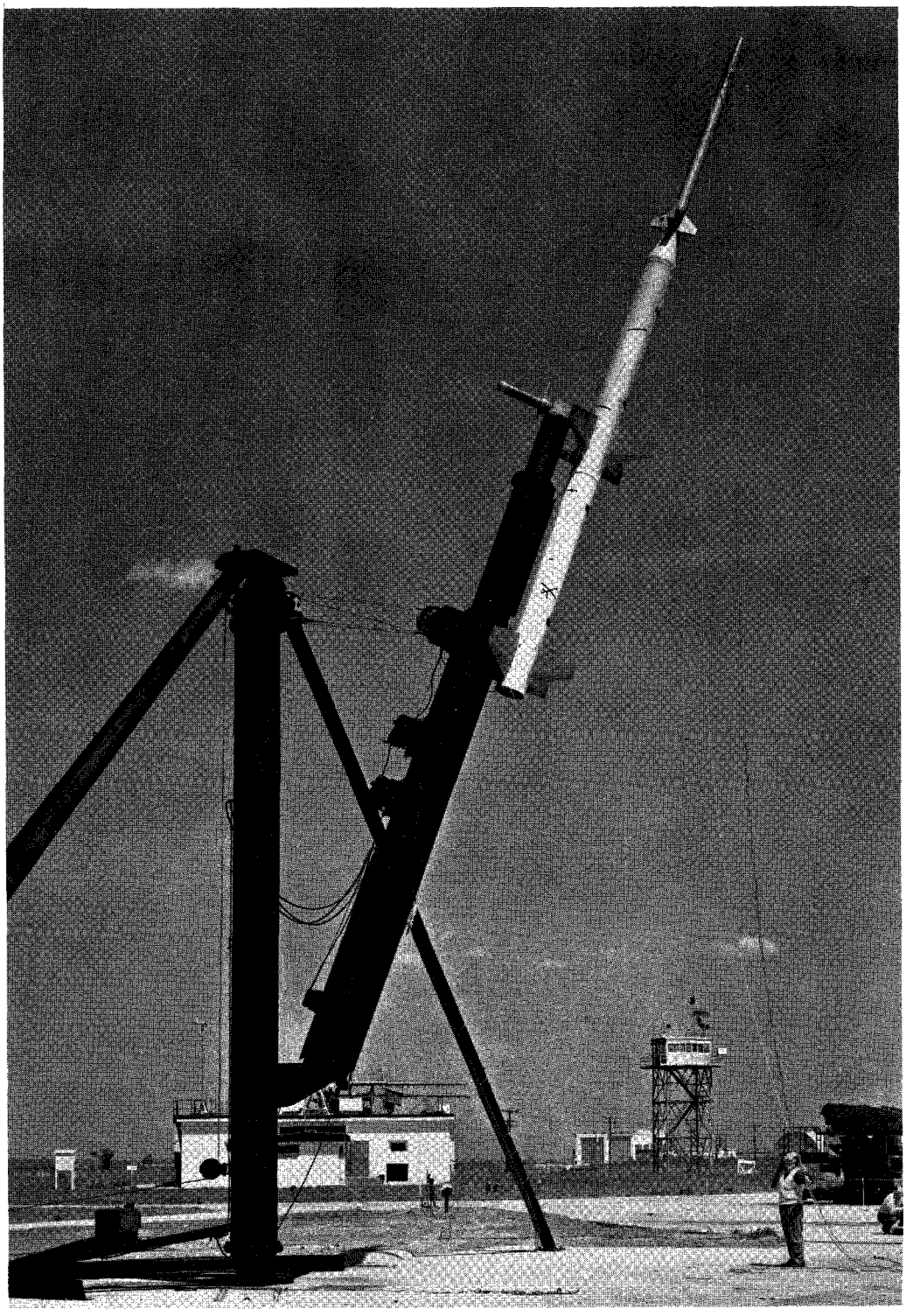

L-59-3527

Figure 3.- Photograph of test vehicle and boosters on launcher.

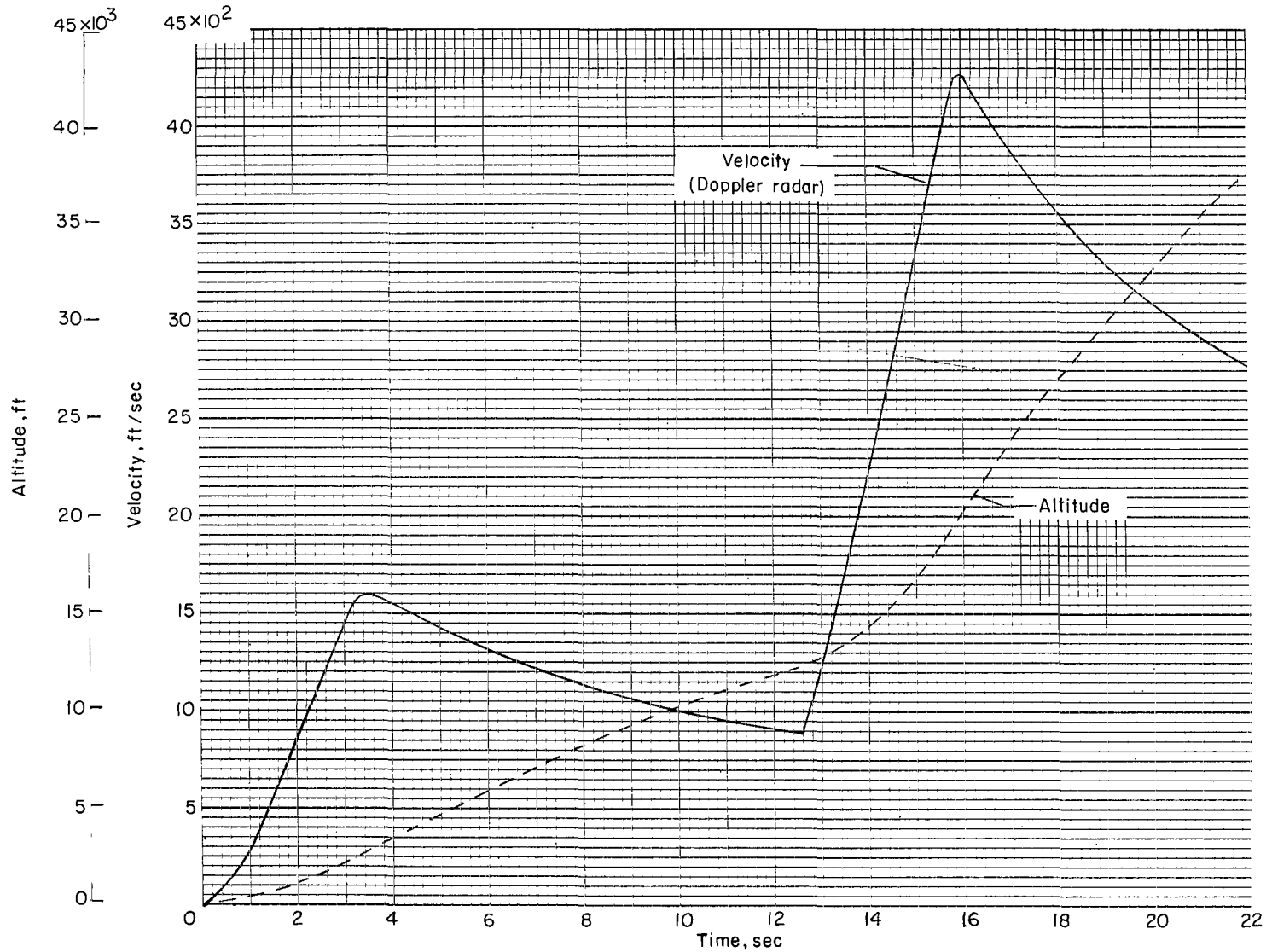

(a) Altitude and velocity.

Figure 4.- Time histories of trajectory data.

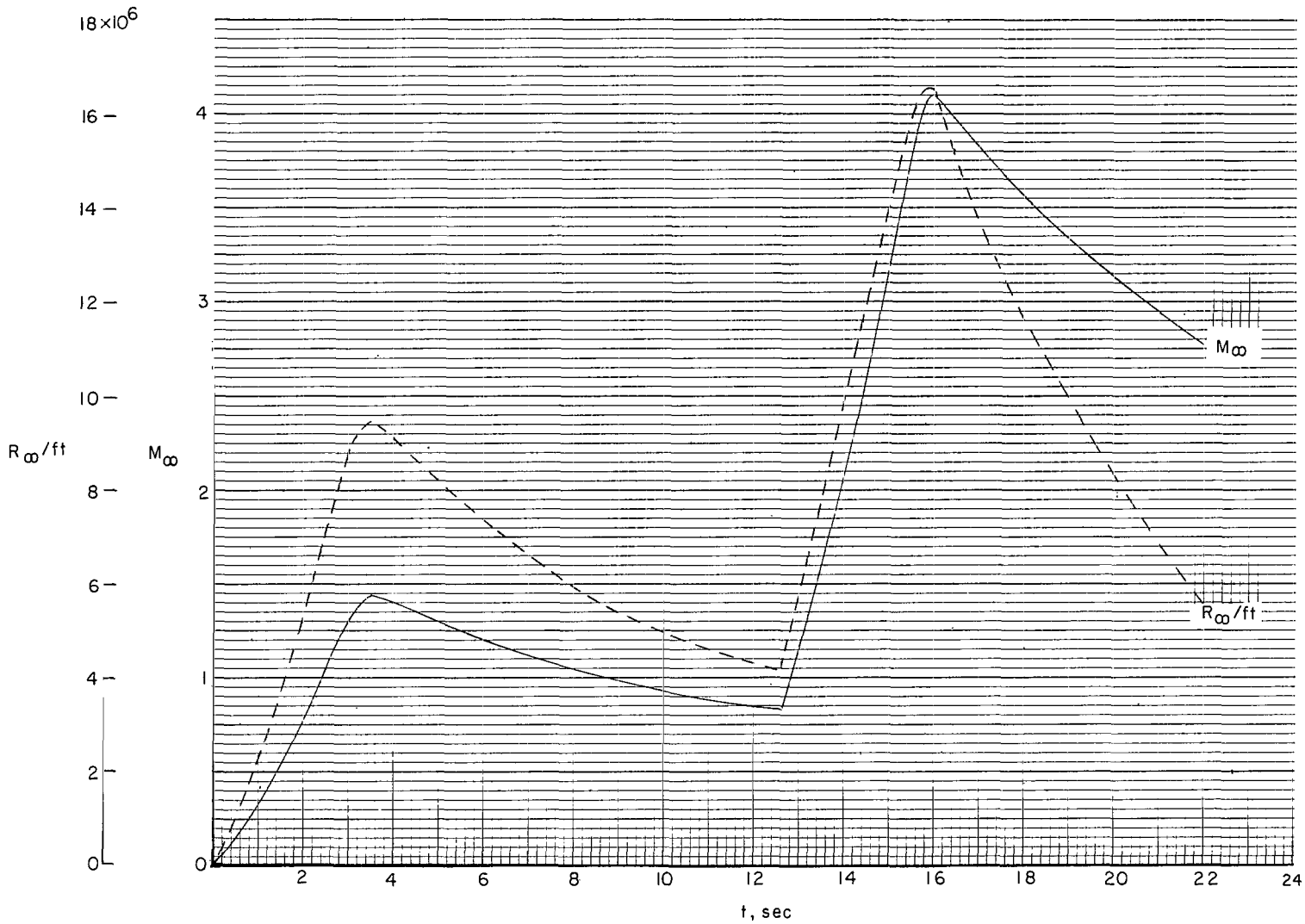

(b) Mach number and Reynolds number per foot.

Figure 4.- Concluded.

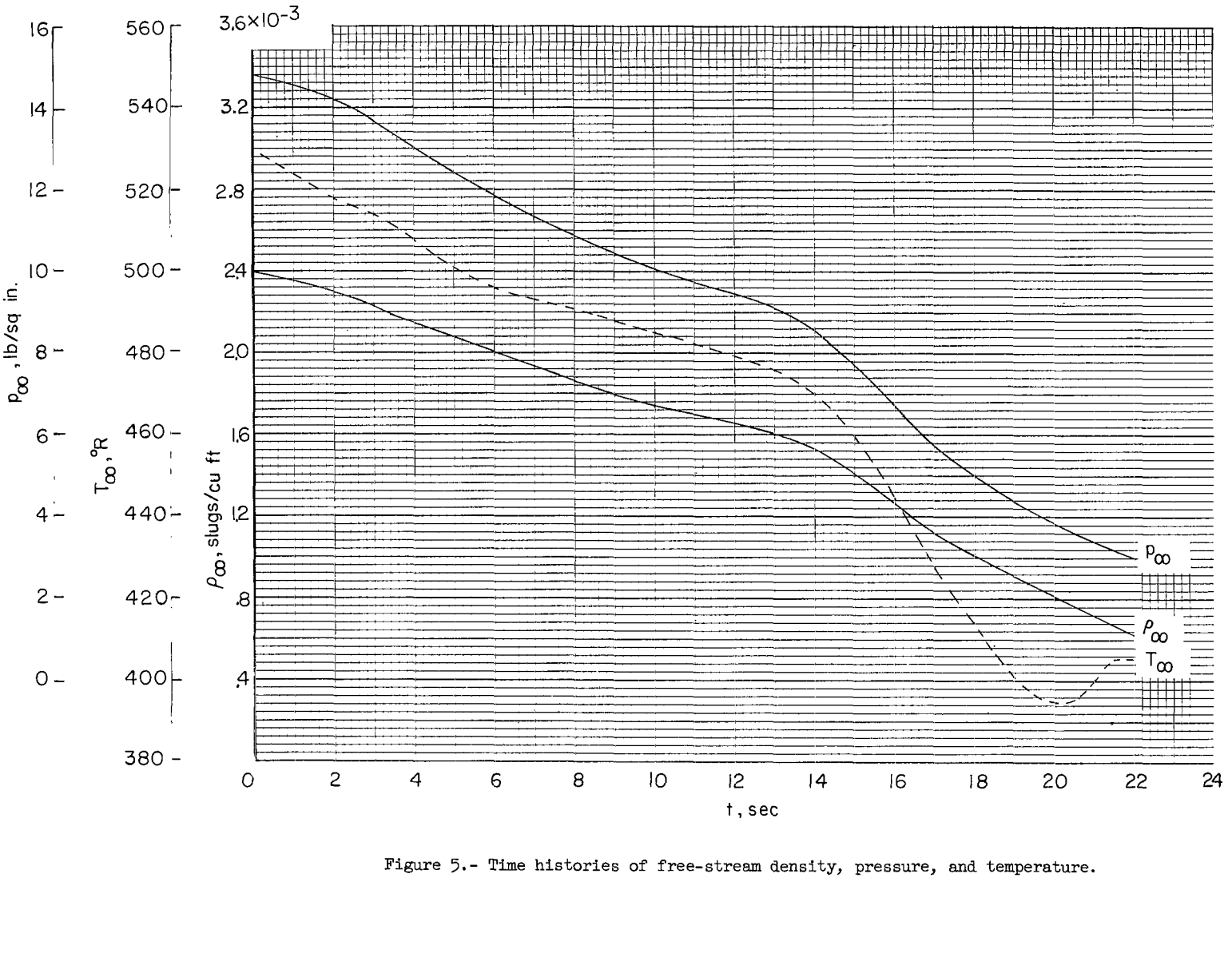

Figure 5.- Time histories of free-stream density, pressure, and temperature.

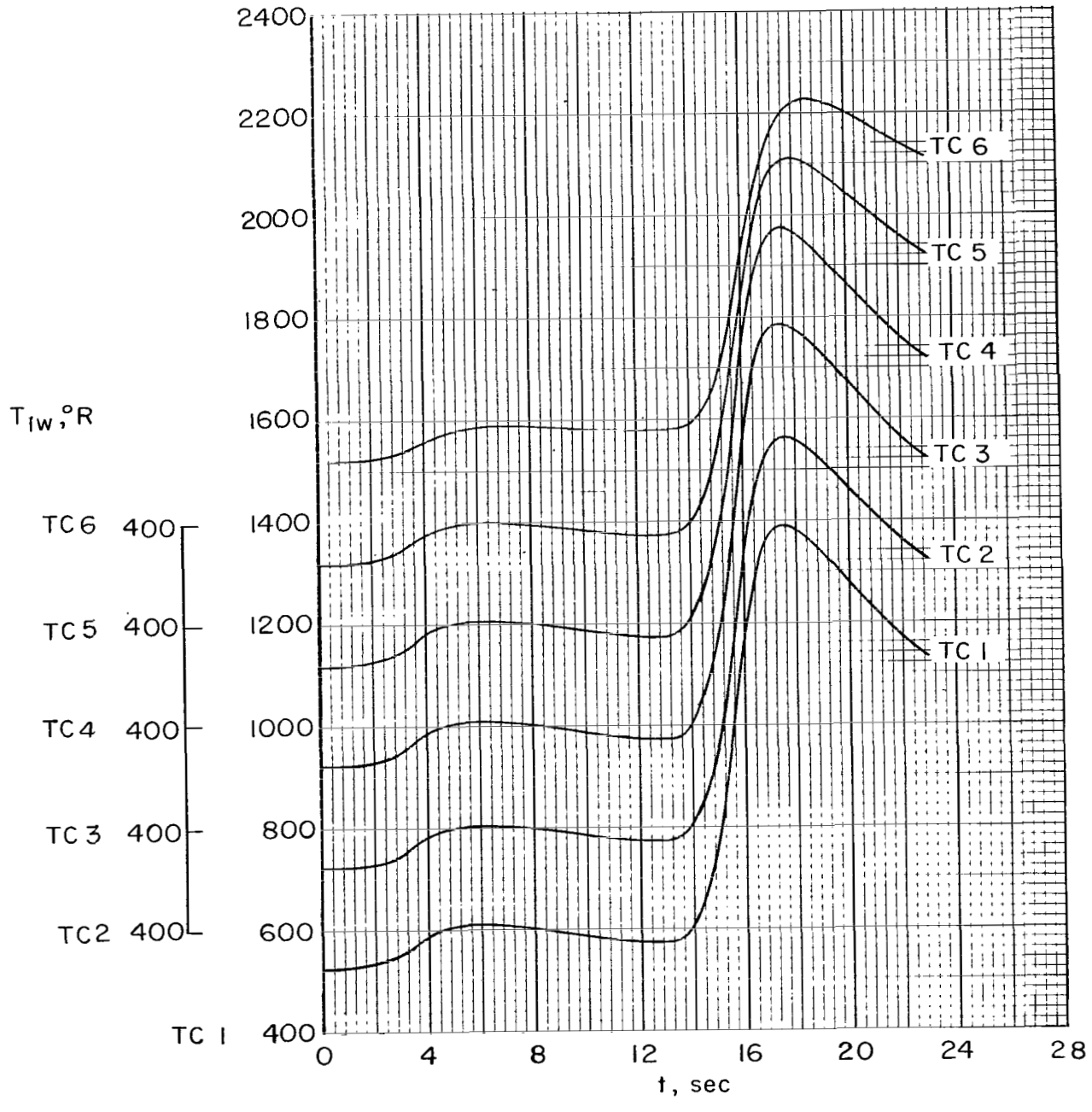

(a) Thermocouples 1 to 6.

Figure 6.- Faired inside surface temperature.

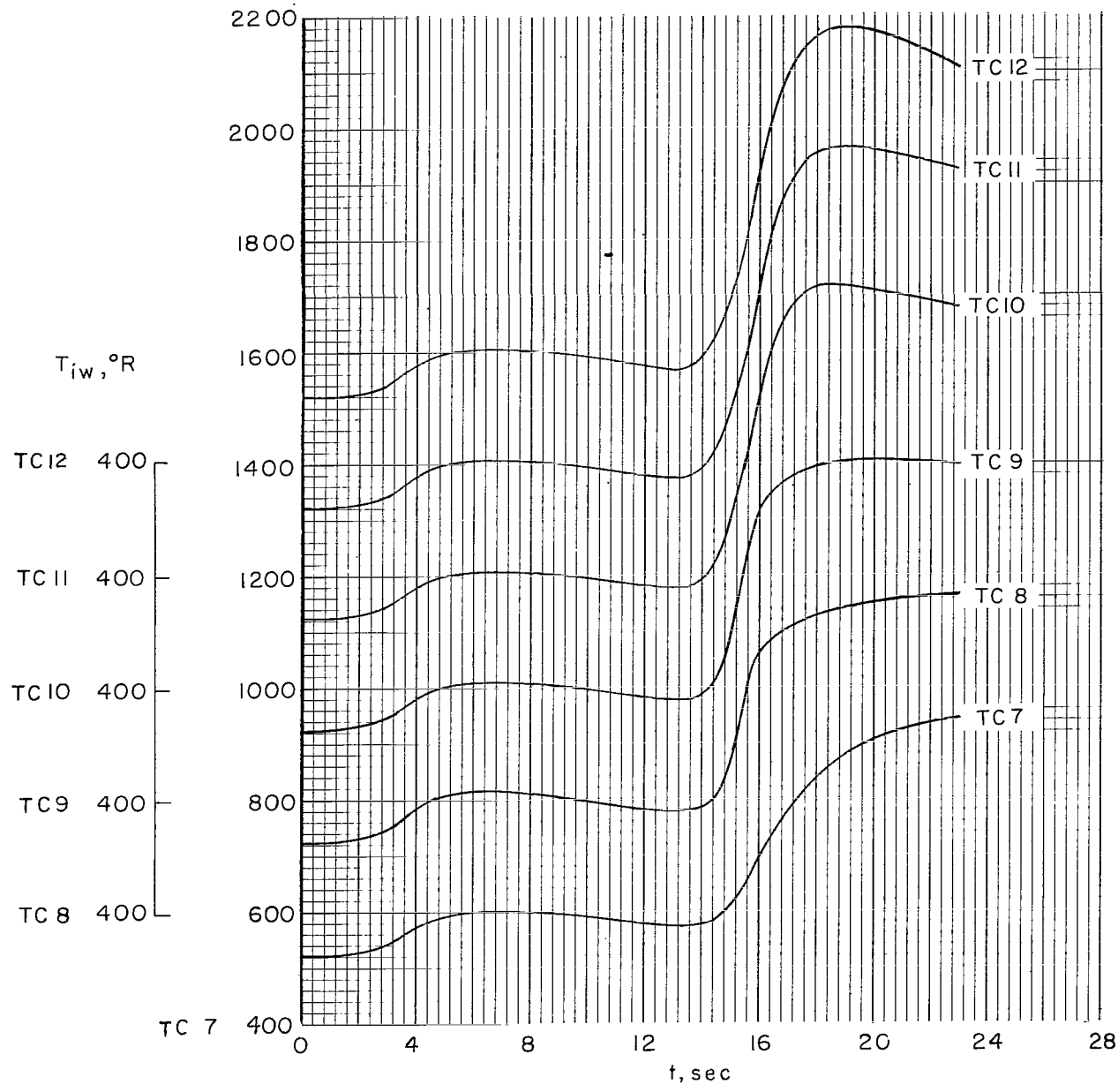

(b) Thermocouples 7 to 12.

Figure 6.- Continued.

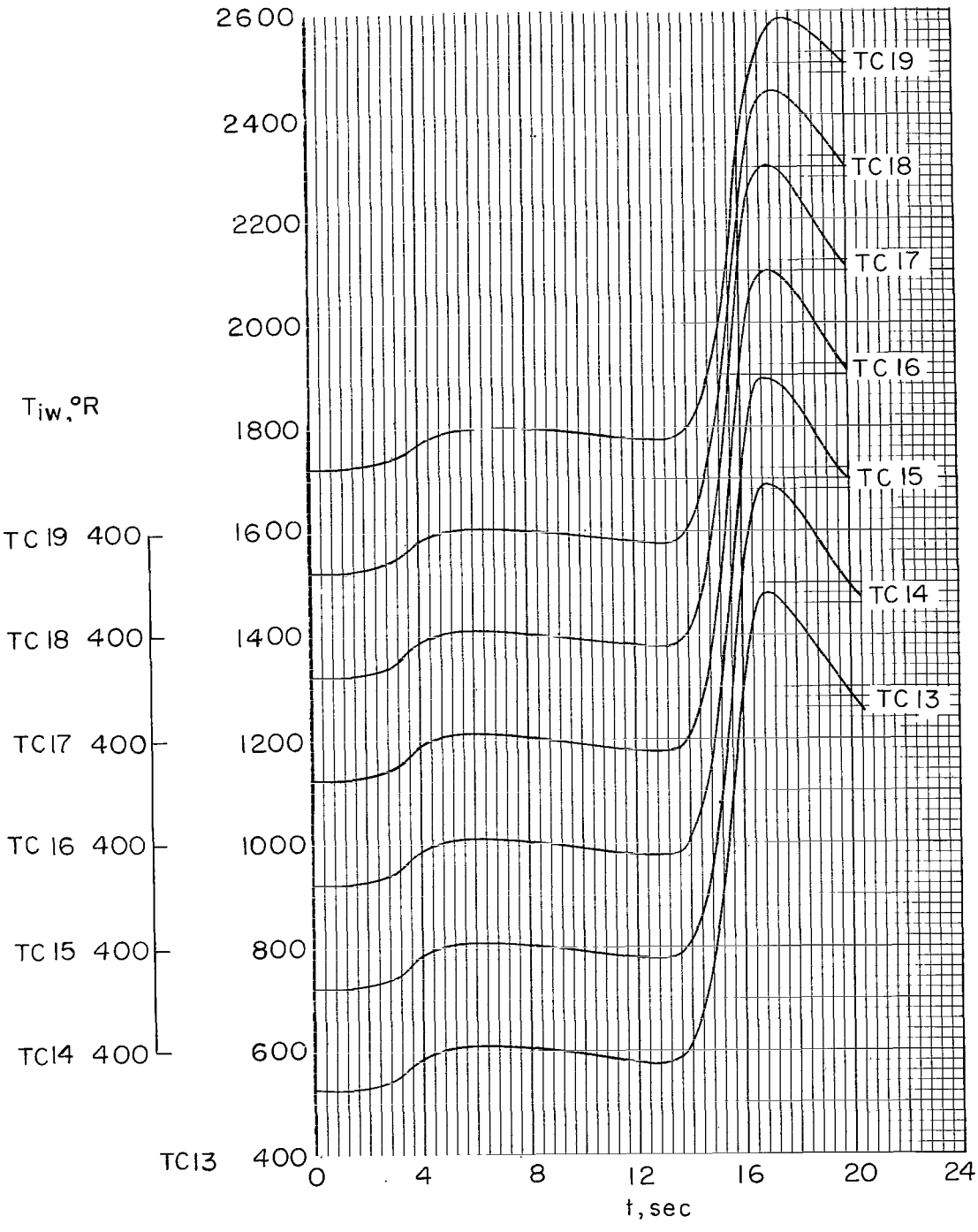

(c) Thermocouples 13 to 19.

Figure 6.- Continued.

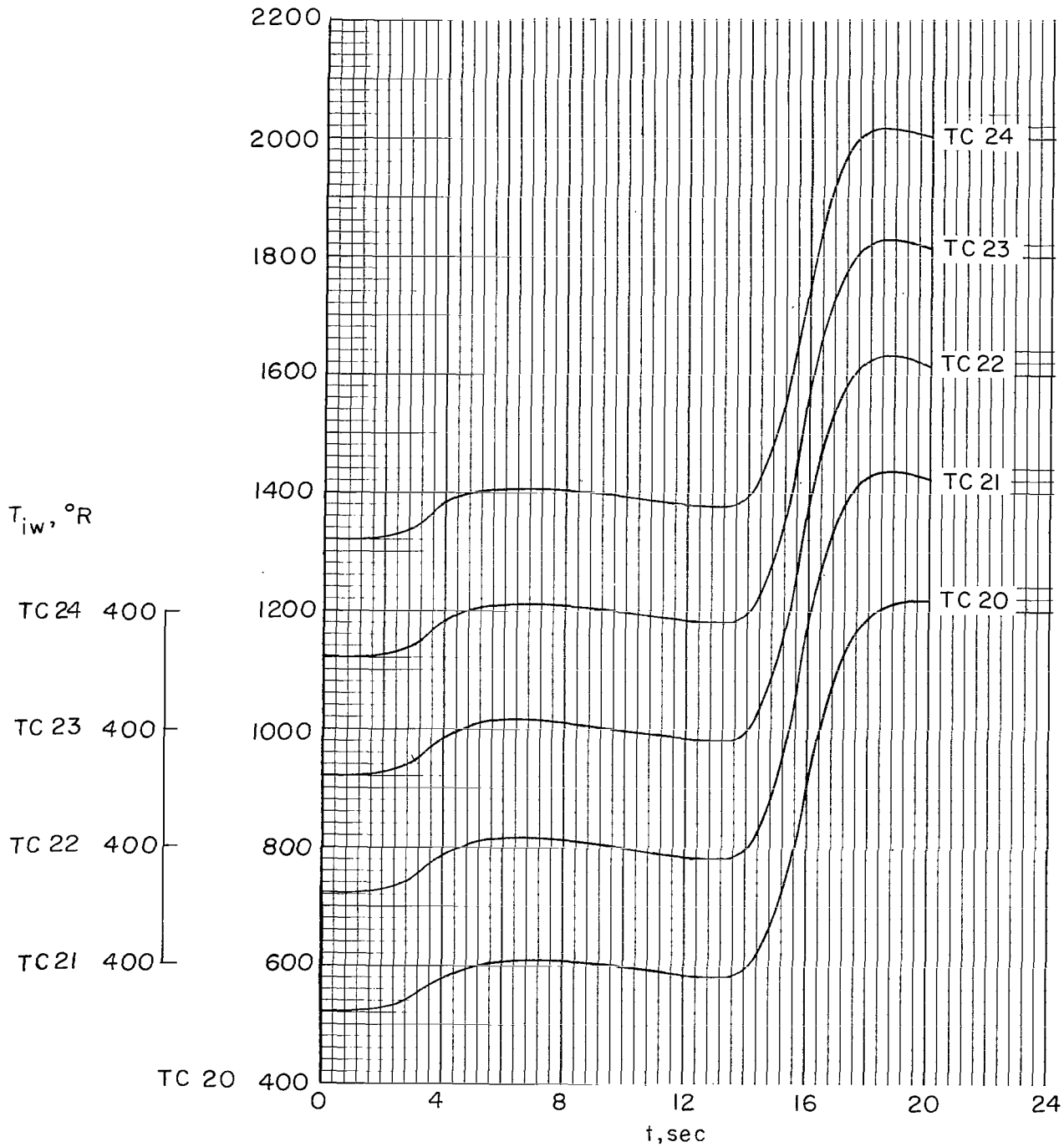

(d) Thermocouples 20 to 24.

Figure 6.- Concluded.

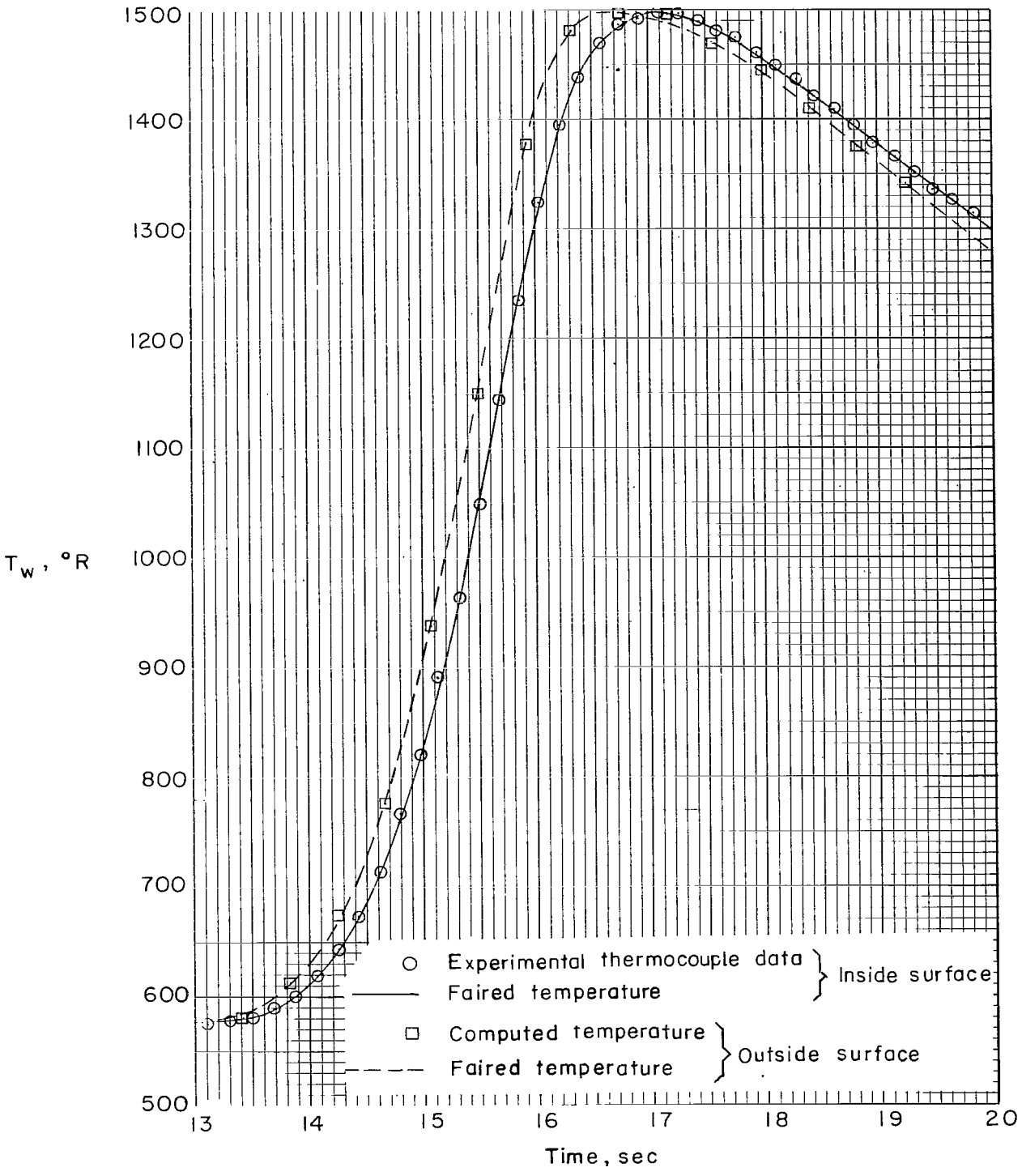

Figure 7.- Typical time history of inside wall and outside wall temperatures.

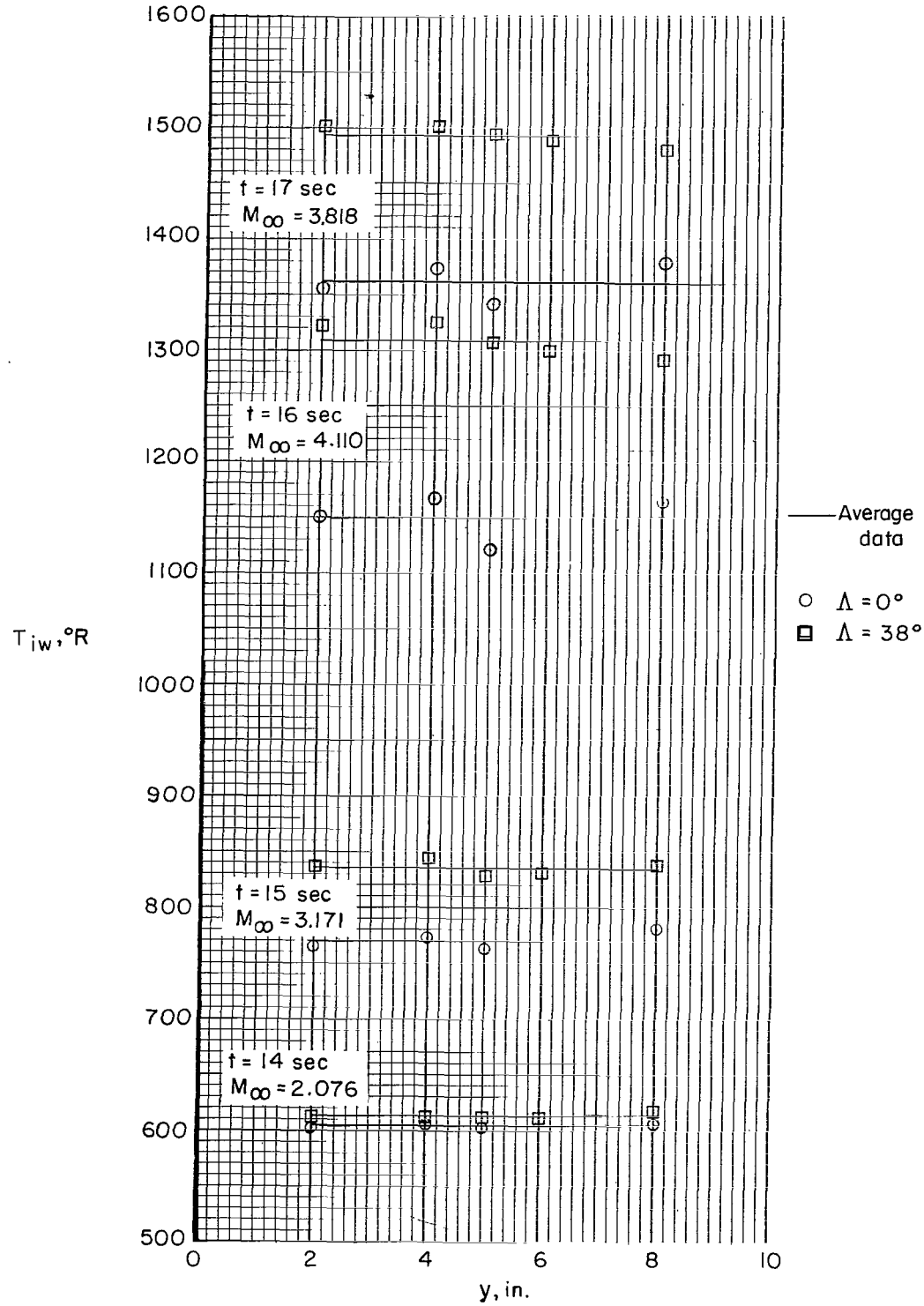

Figure 8.- Stagnation-line spanwise temperature distributions on swept and unswept fins.

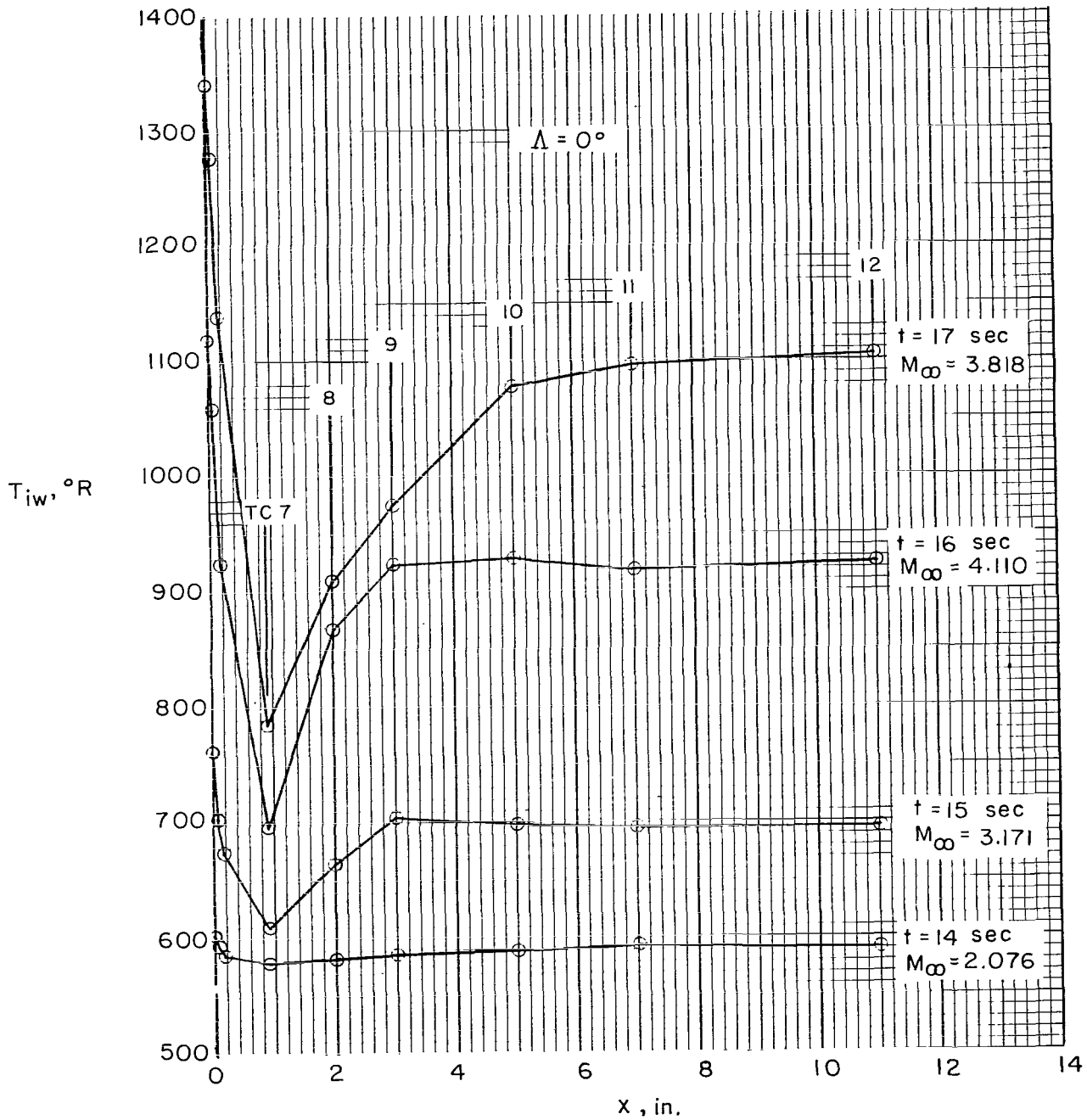

(a) Unswept fin.

Figure 9.- Chordwise temperature distributions.

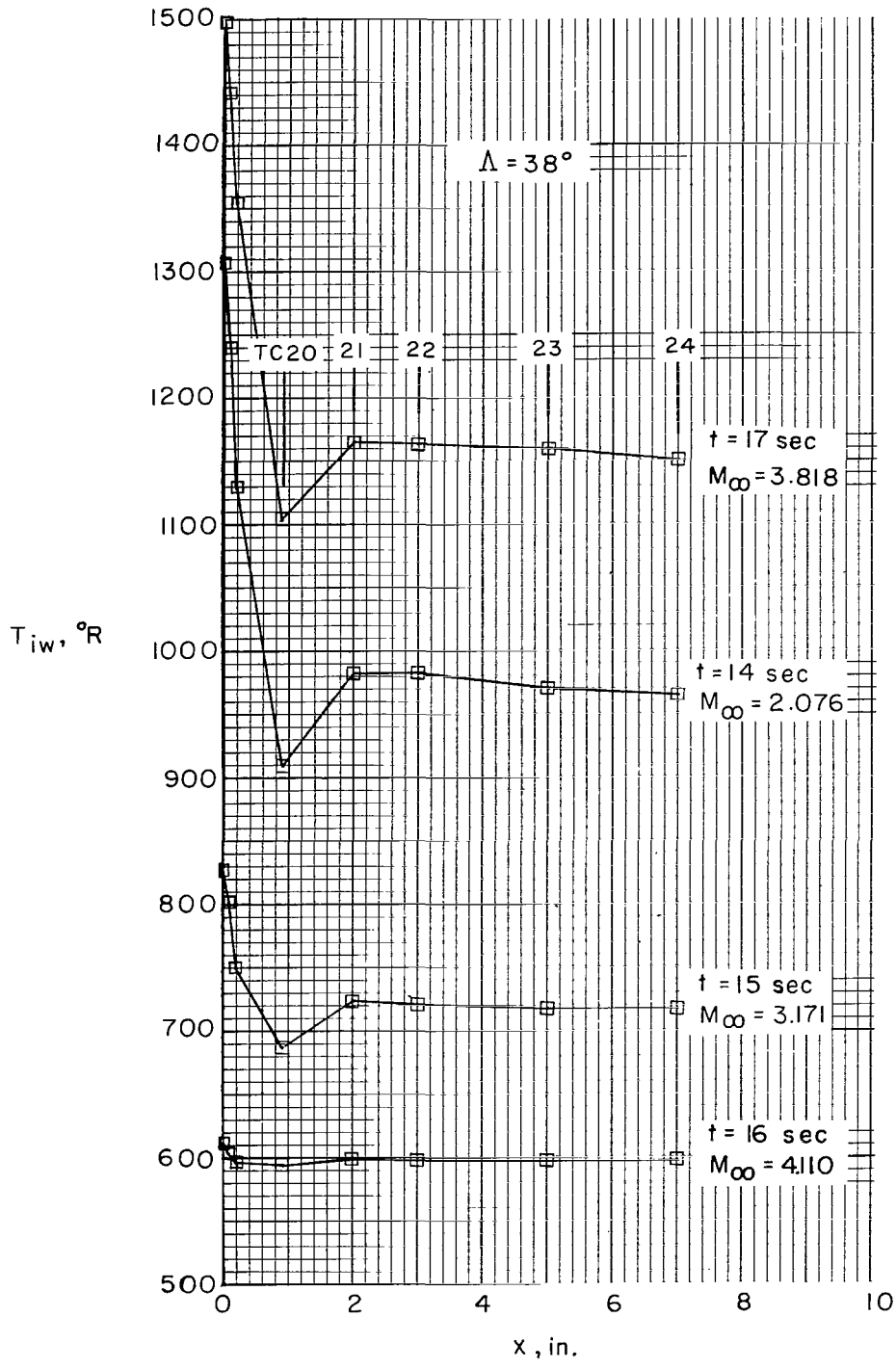

(b) Swept fin.

Figure 9.- Concluded.

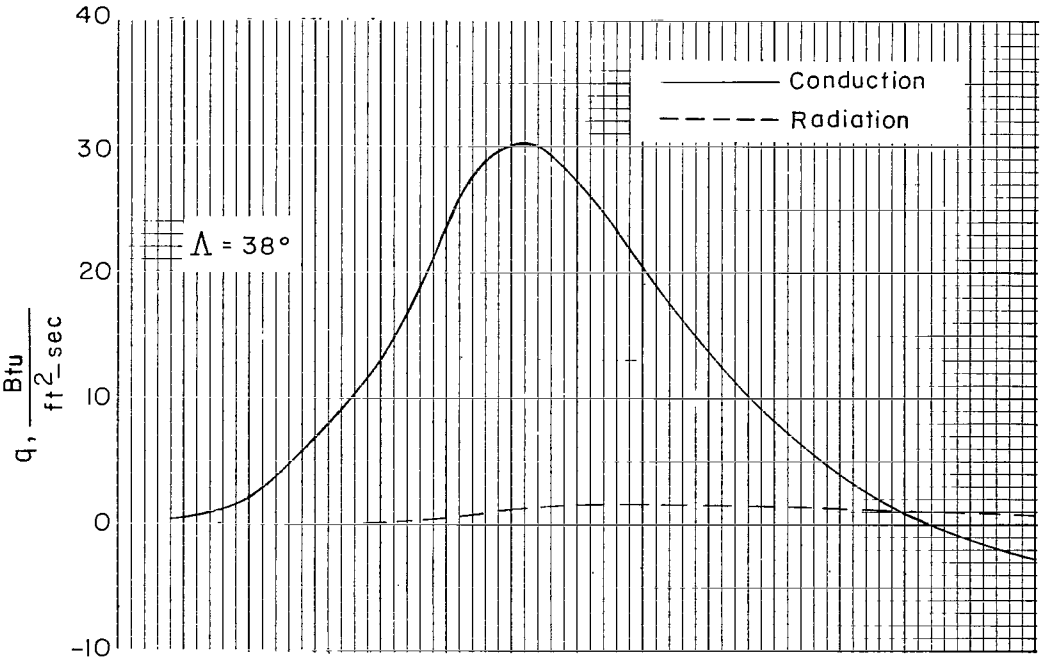

(a) Swept fin.

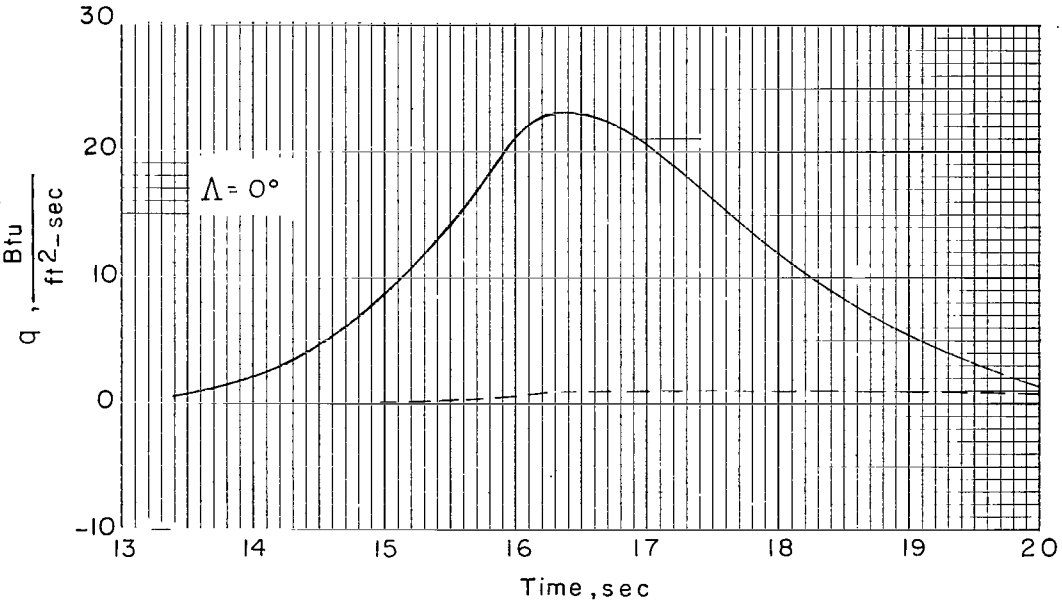

(b) Unswept fin.

Figure 10.- Corrections for conduction and radiation at stagnation line.

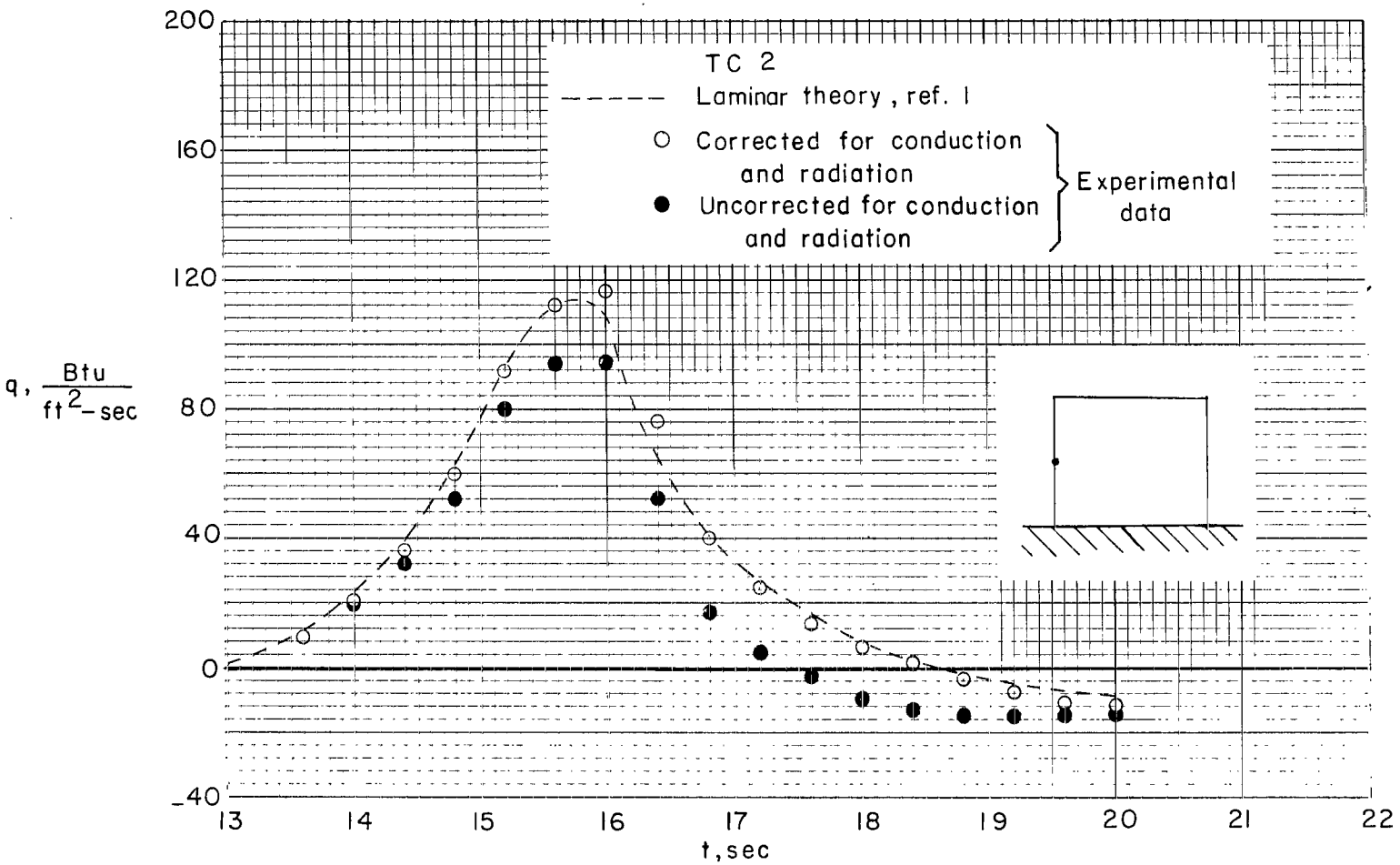

(a) Unswept fin.

Figure 11.- Experimental stagnation-line heat-transfer rates at midspan station.

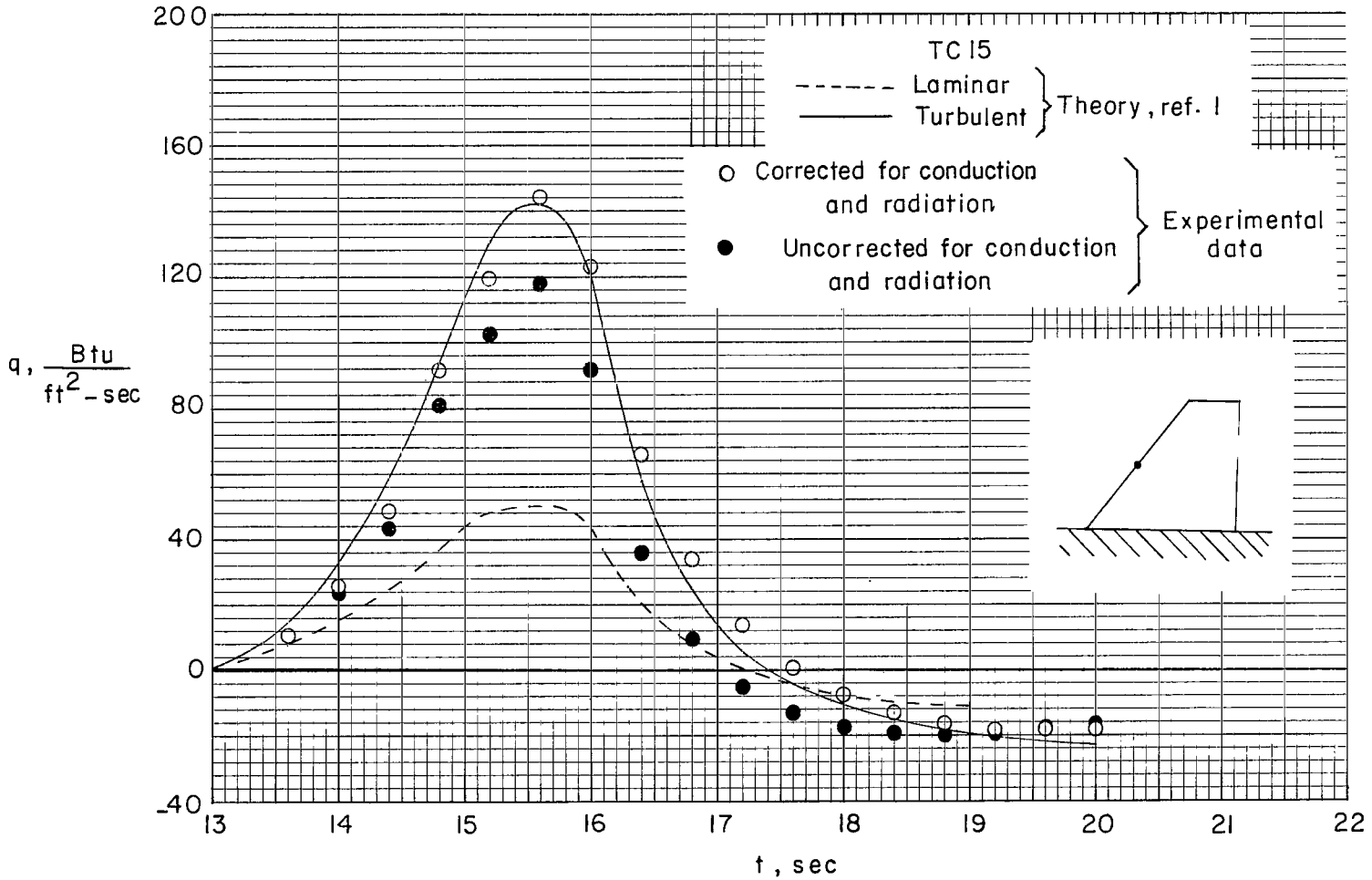

(b) Swept fin.

Figure 11.- Concluded.

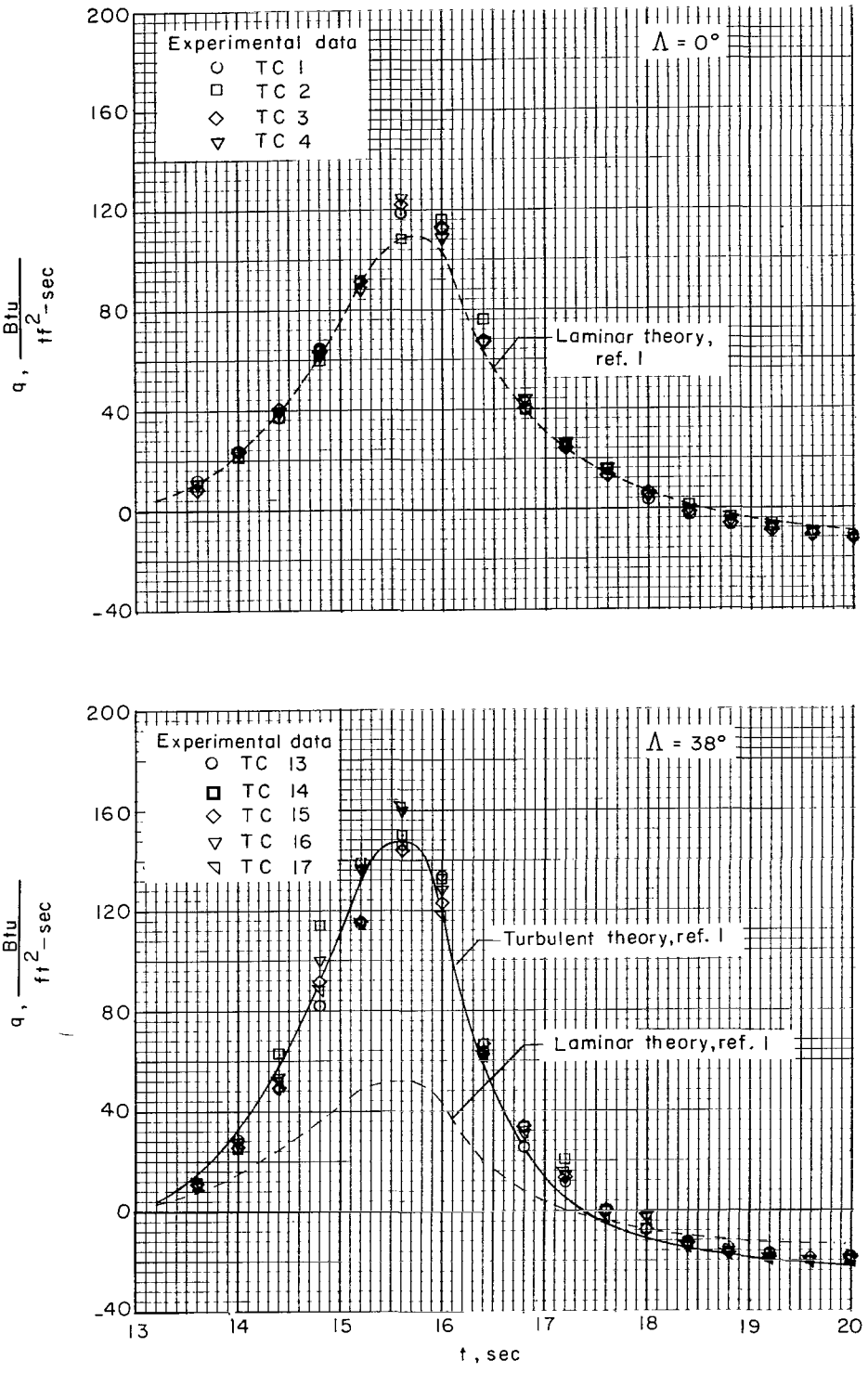

Figure 12.- Experimental stagnation-line heat-transfer rates compared with theory.

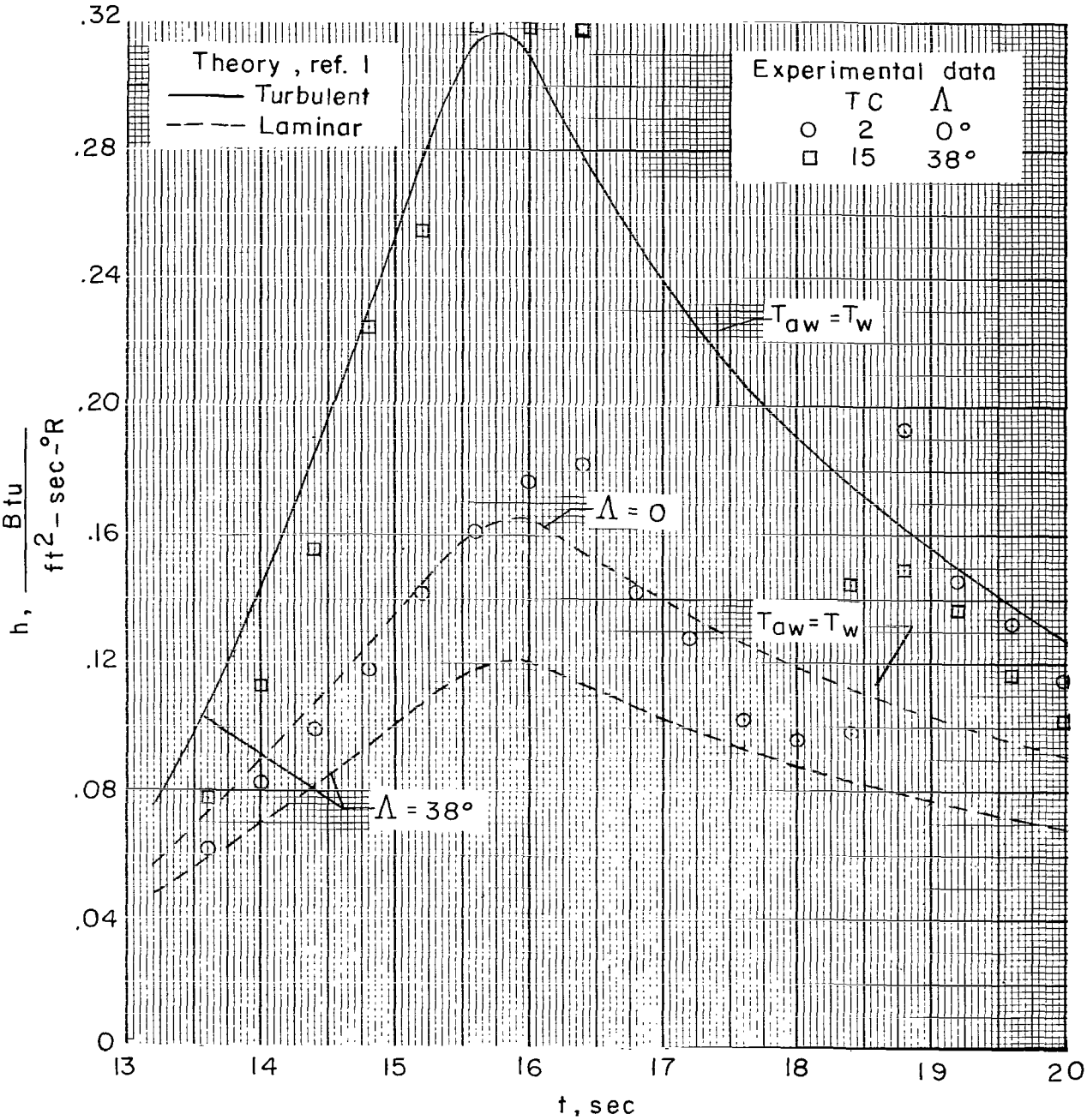

Figure 13.- Effect of sweep angle on stagnation-line heat-transfer coefficient.

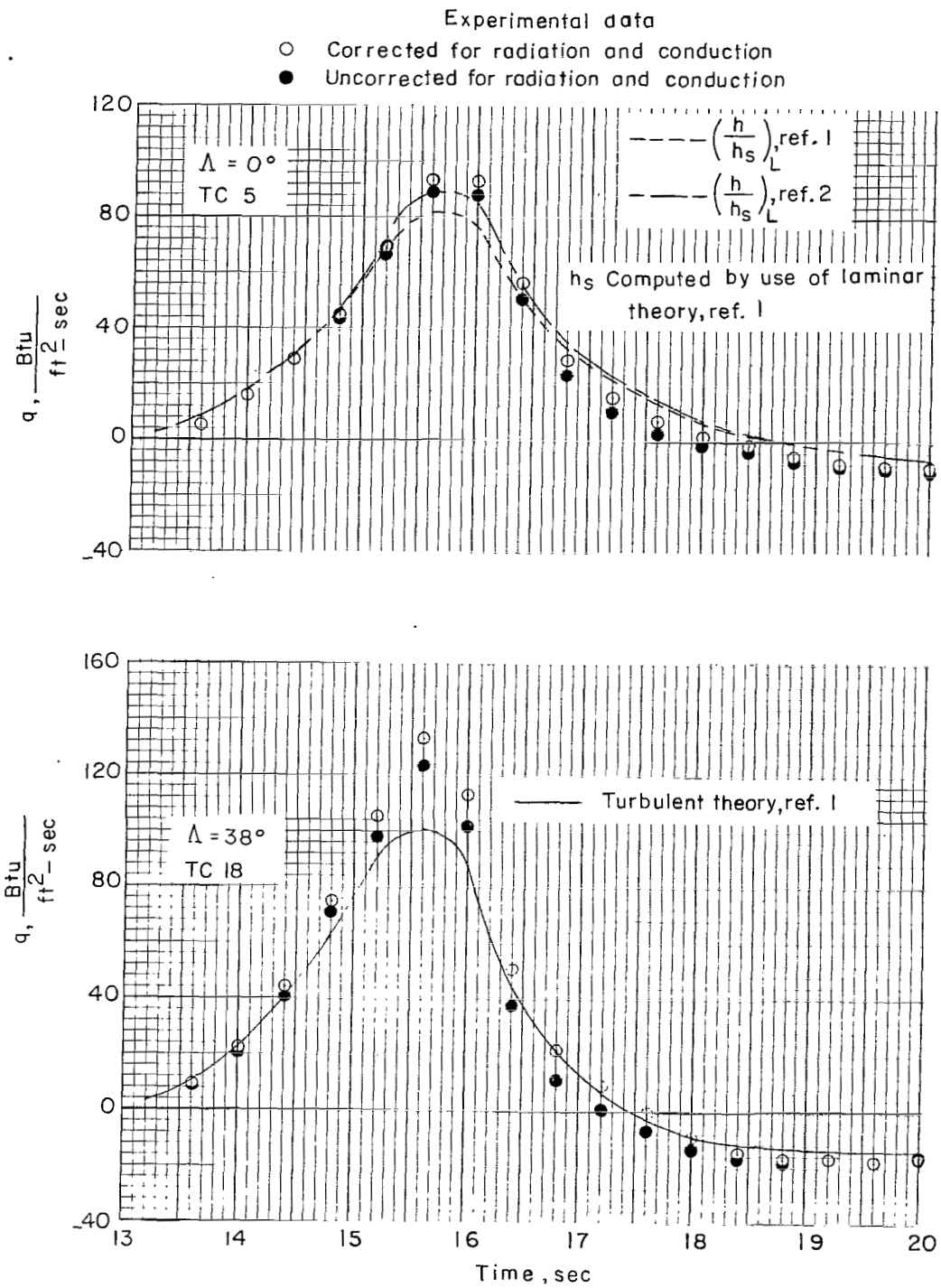

(a) $\theta = 45^{\circ}$.

Figure 14.- Heat transfer on cylindrical sections.

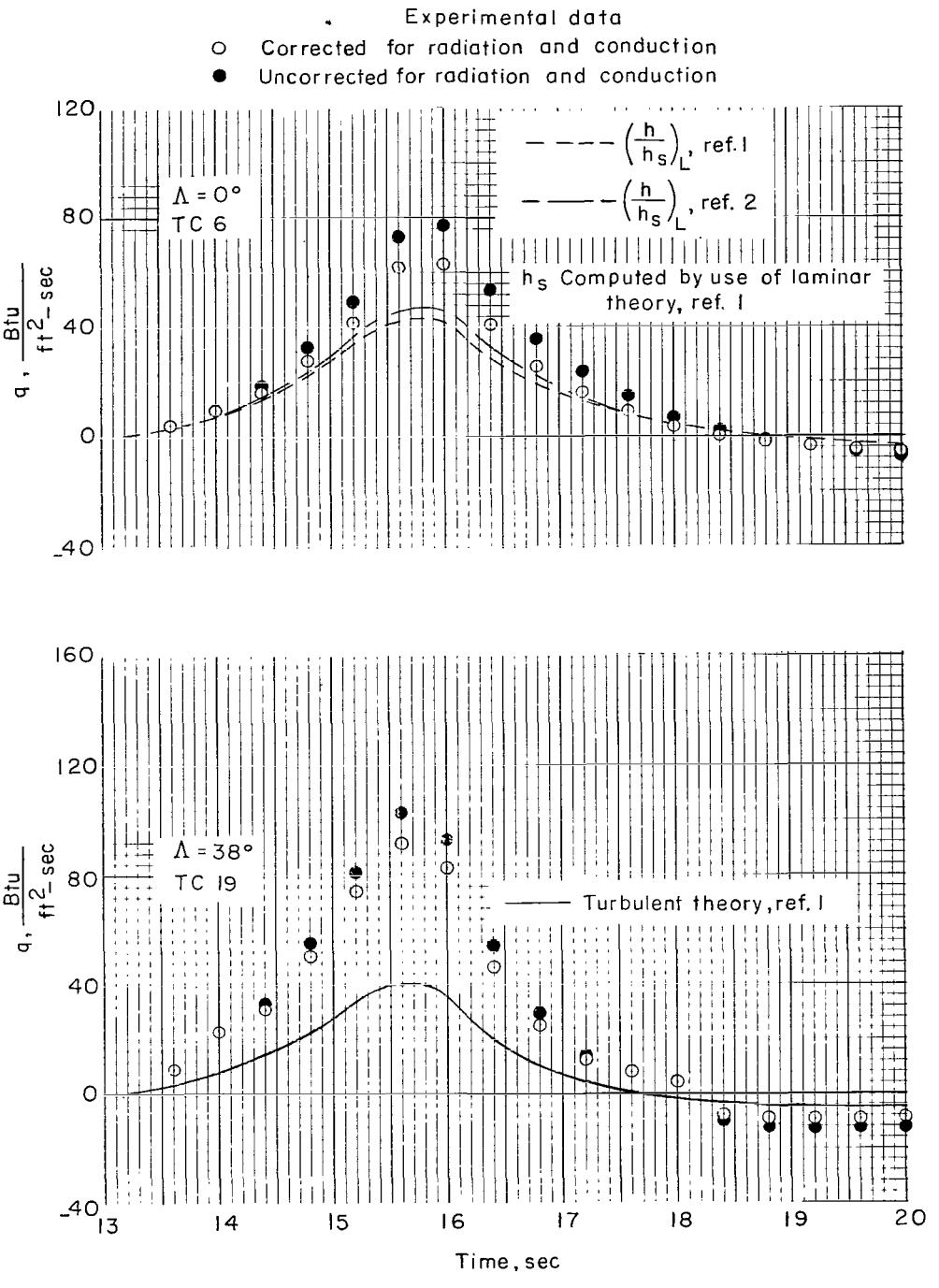

(b) Tangency point.

Figure 14.- Concluded.

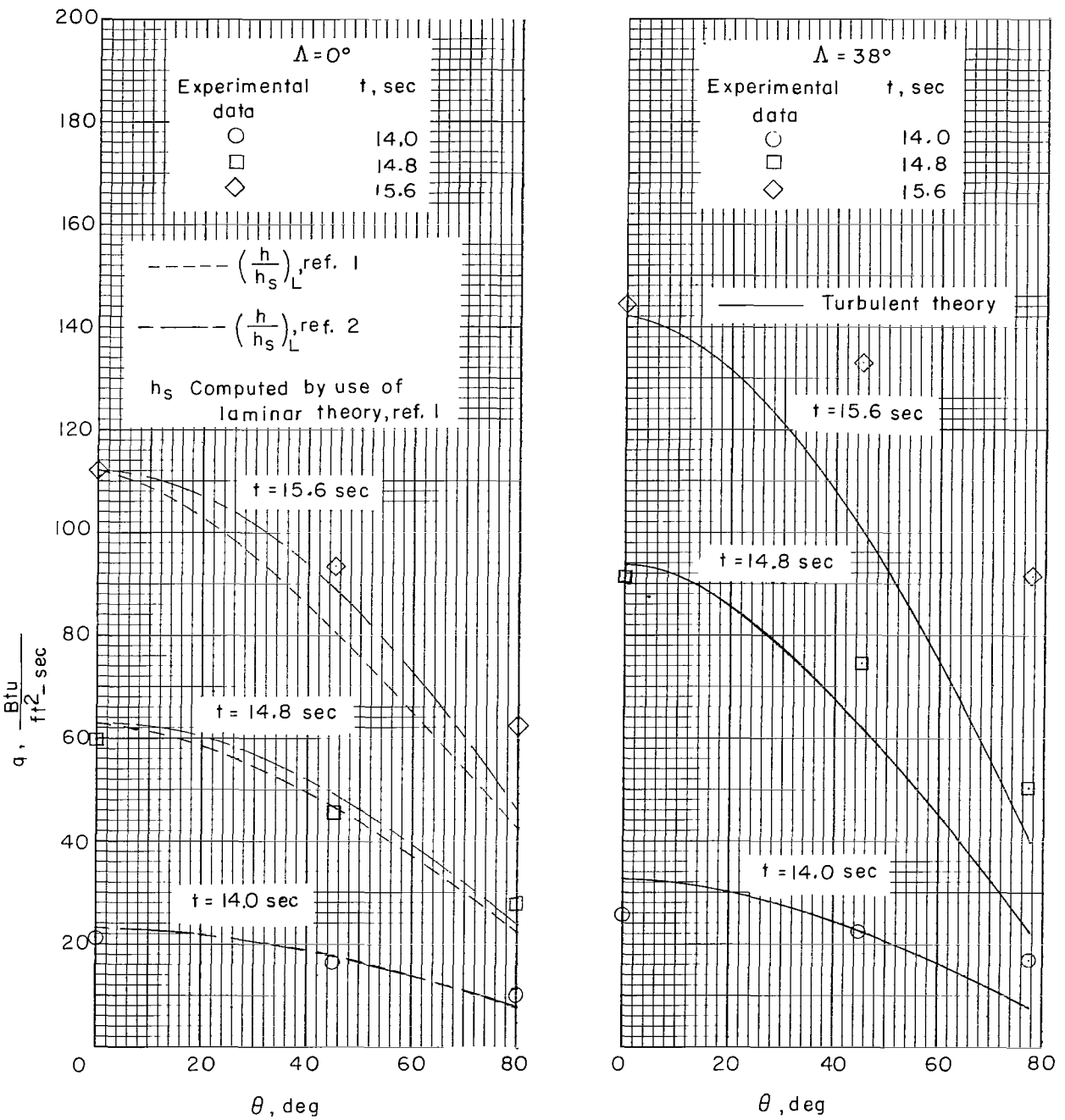

Figure 15.- Distribution of heat transfer on cylindrical sections.

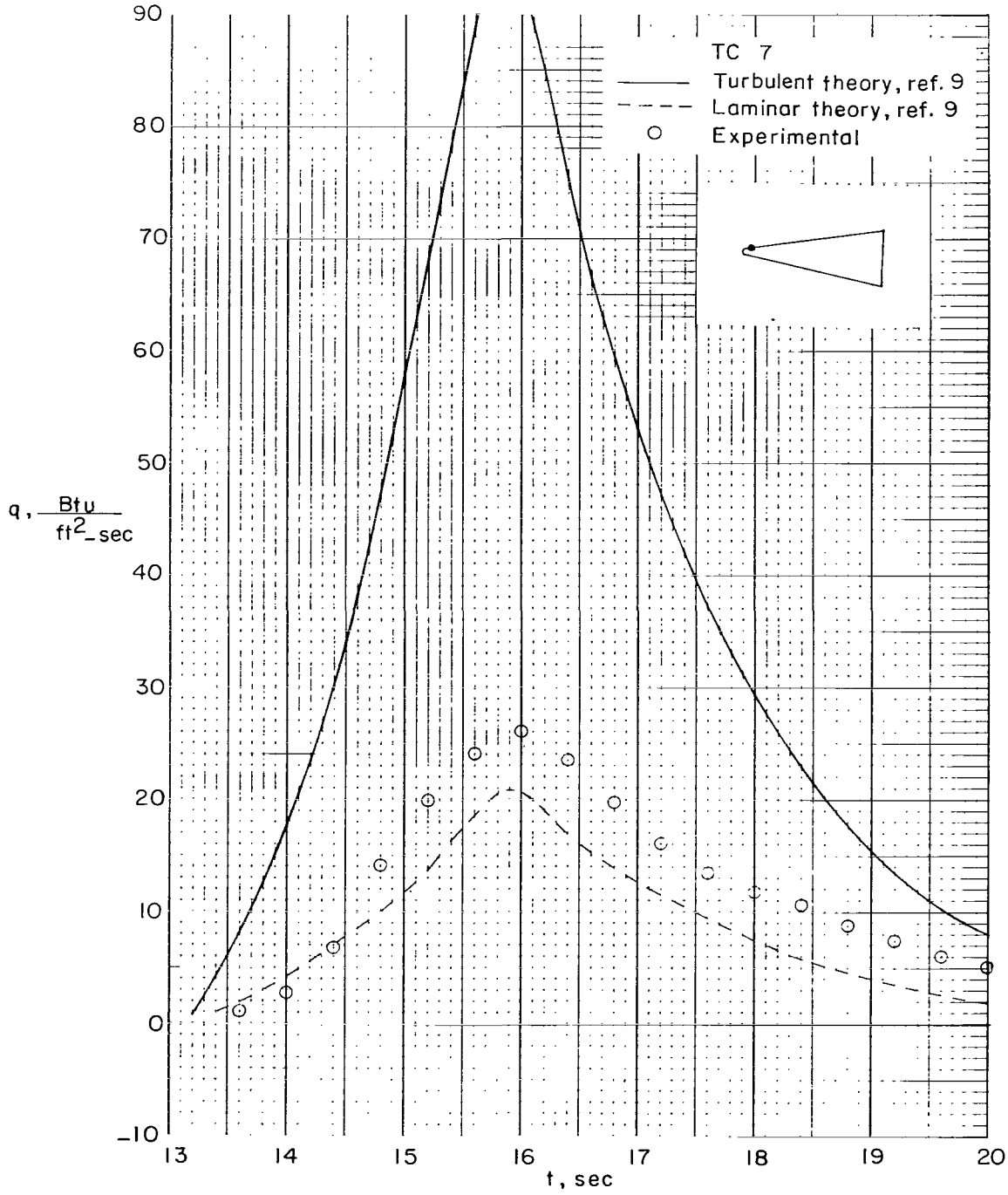

(a) Thermocouple 7.

Figure 16.- Heat transfer on wedge section of unswept fin.

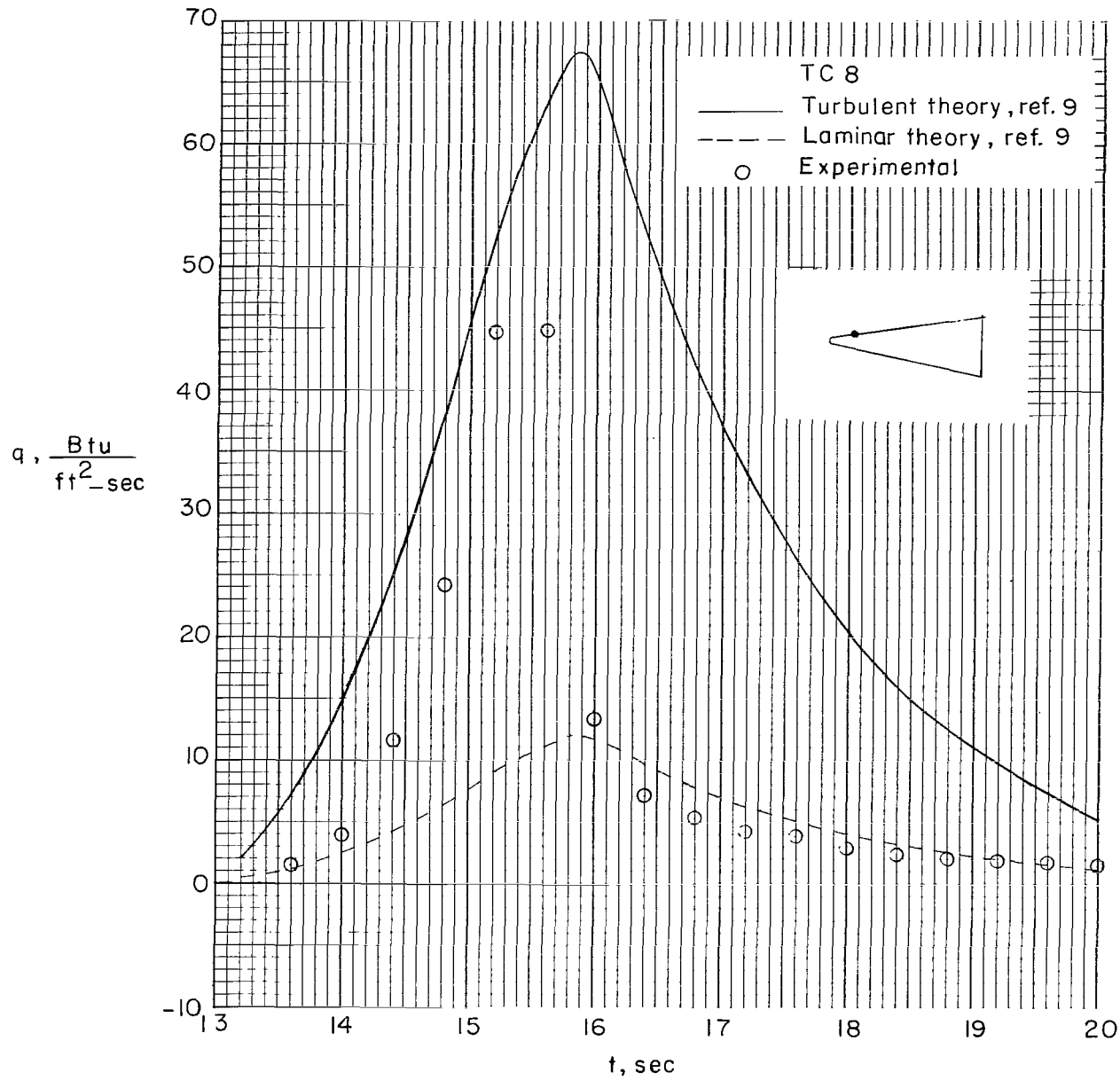

(b) Thermocouple 8.

Figure 16.- Continued.

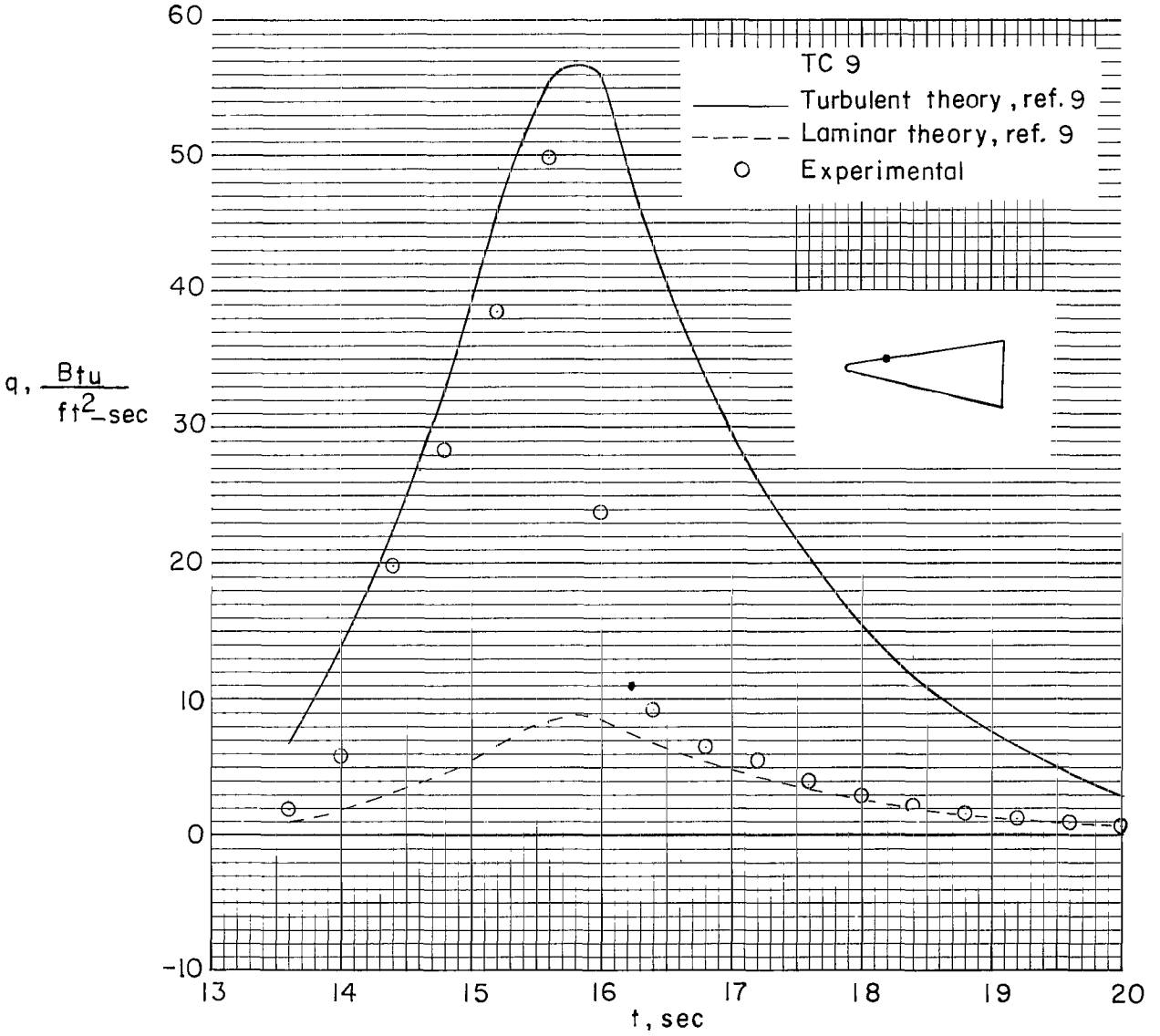

(c) Thermocouple 9.

Figure 16.- Continued.

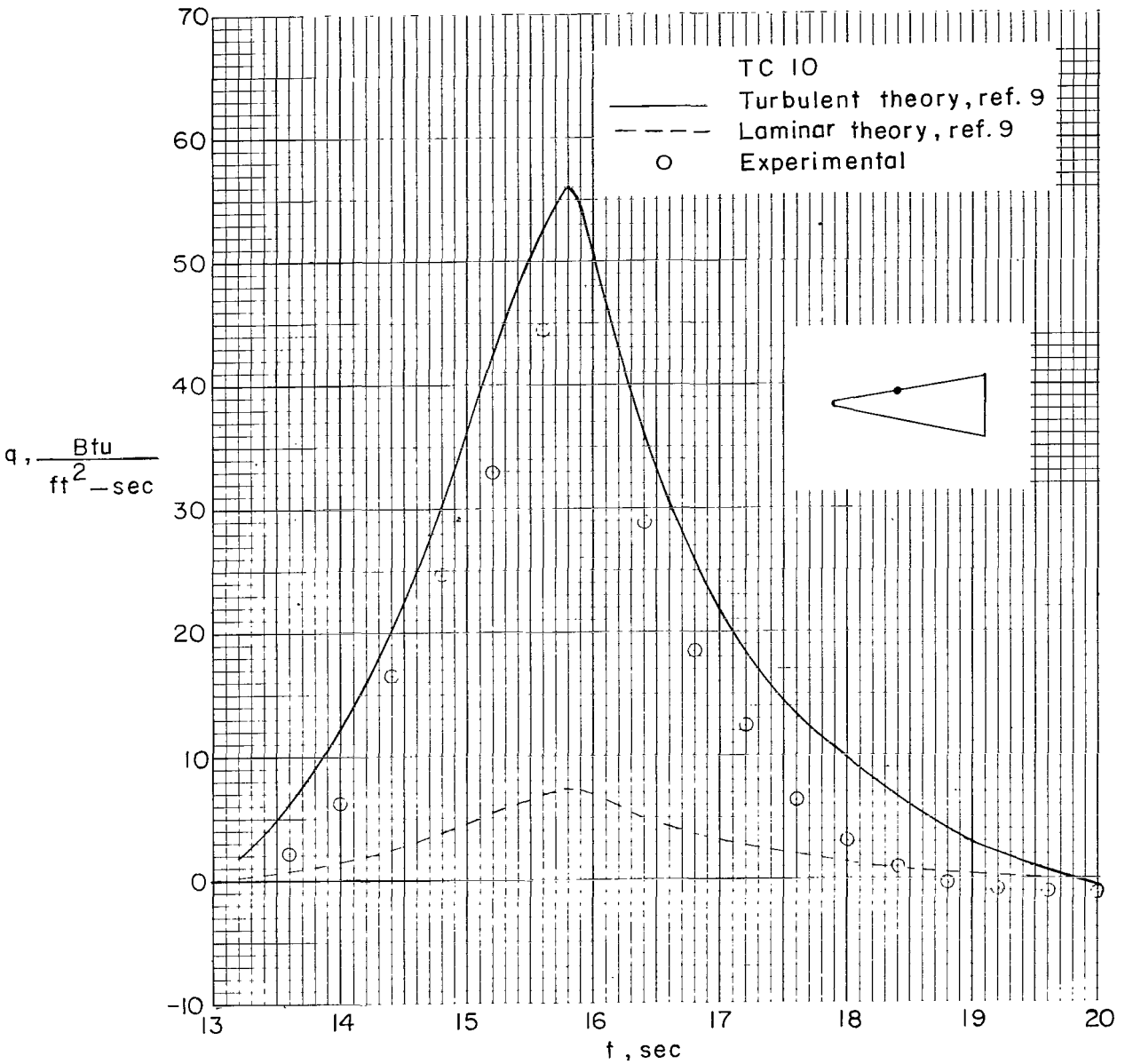

(d) Thermocouple 10.

Figure 16.- Continued.

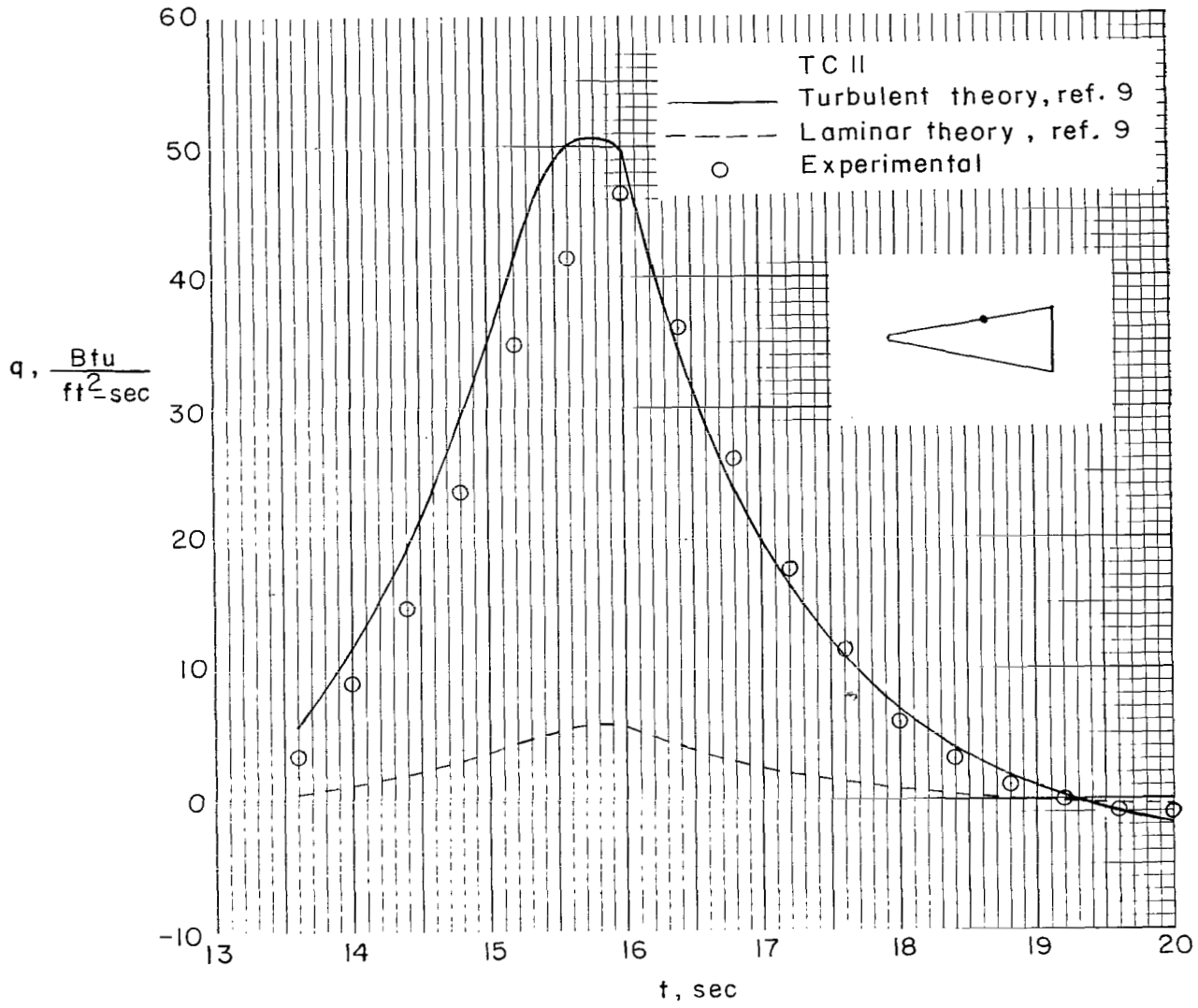

(e) Thermocouple 11.

Figure 16.- Continued.

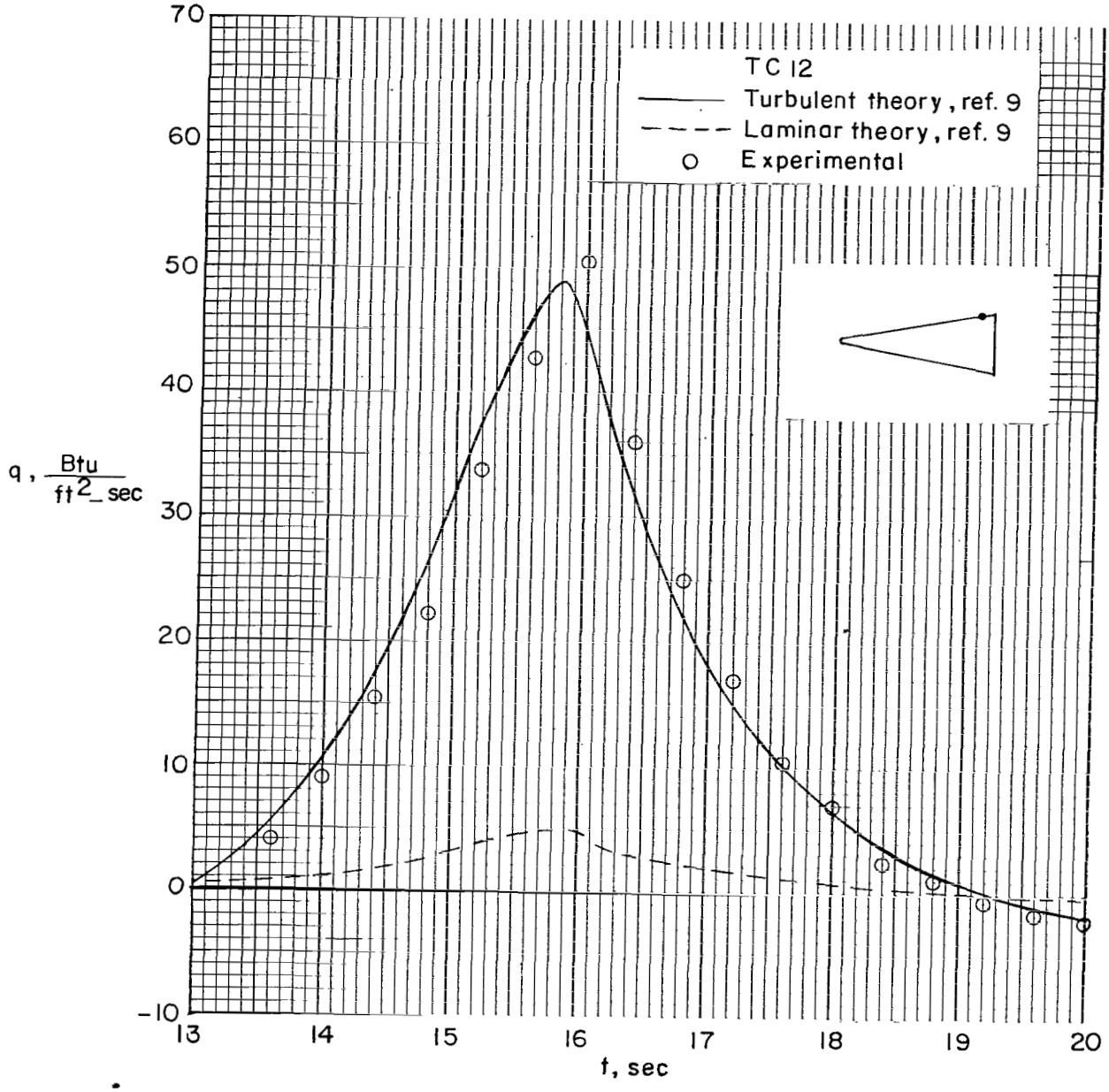

(f) Thermocouple 12.

Figure 16.- Concluded.

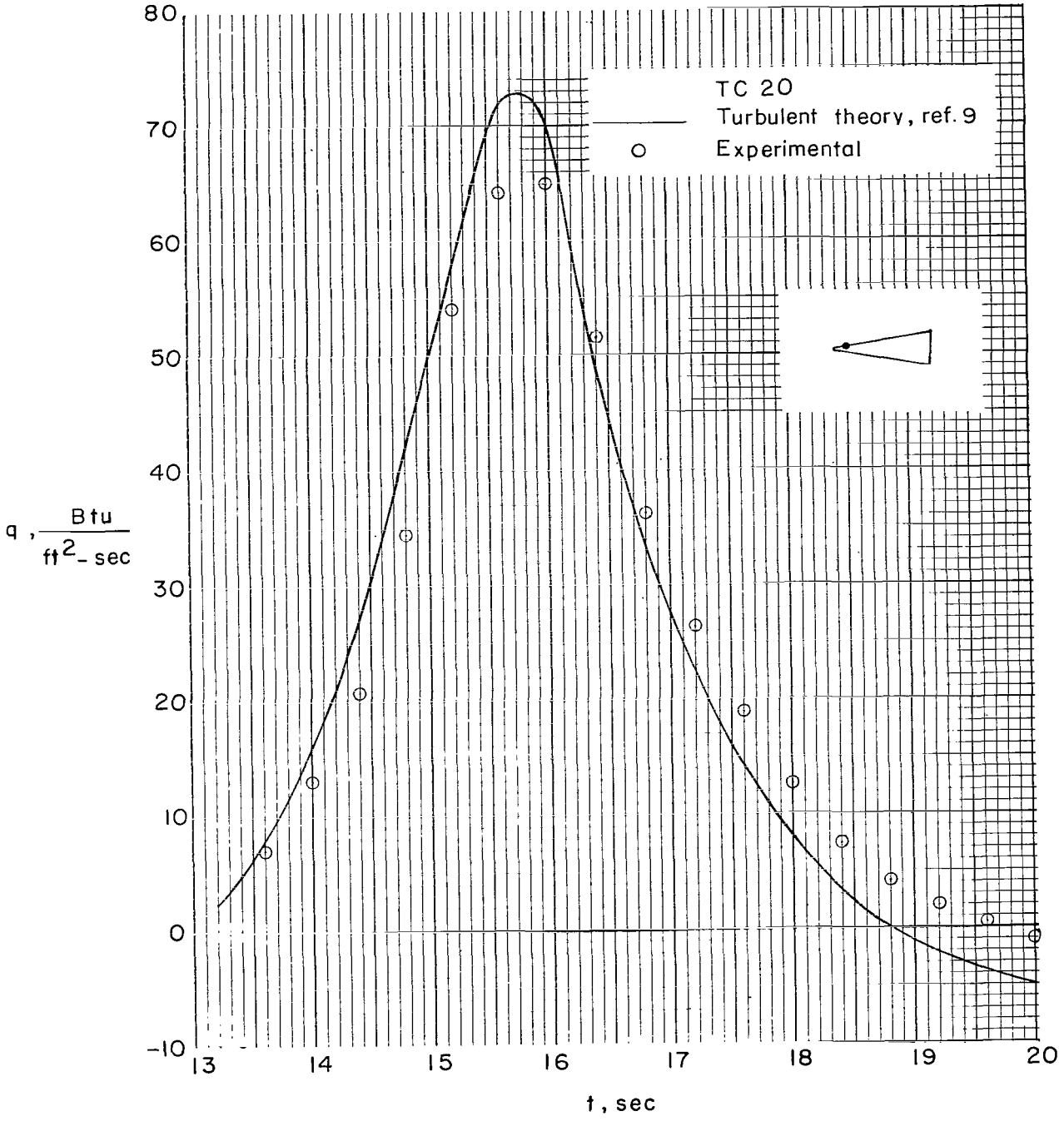

(a) Thermocouple 20.

Figure 17.- Heat transfer on wedge section of swept fin.

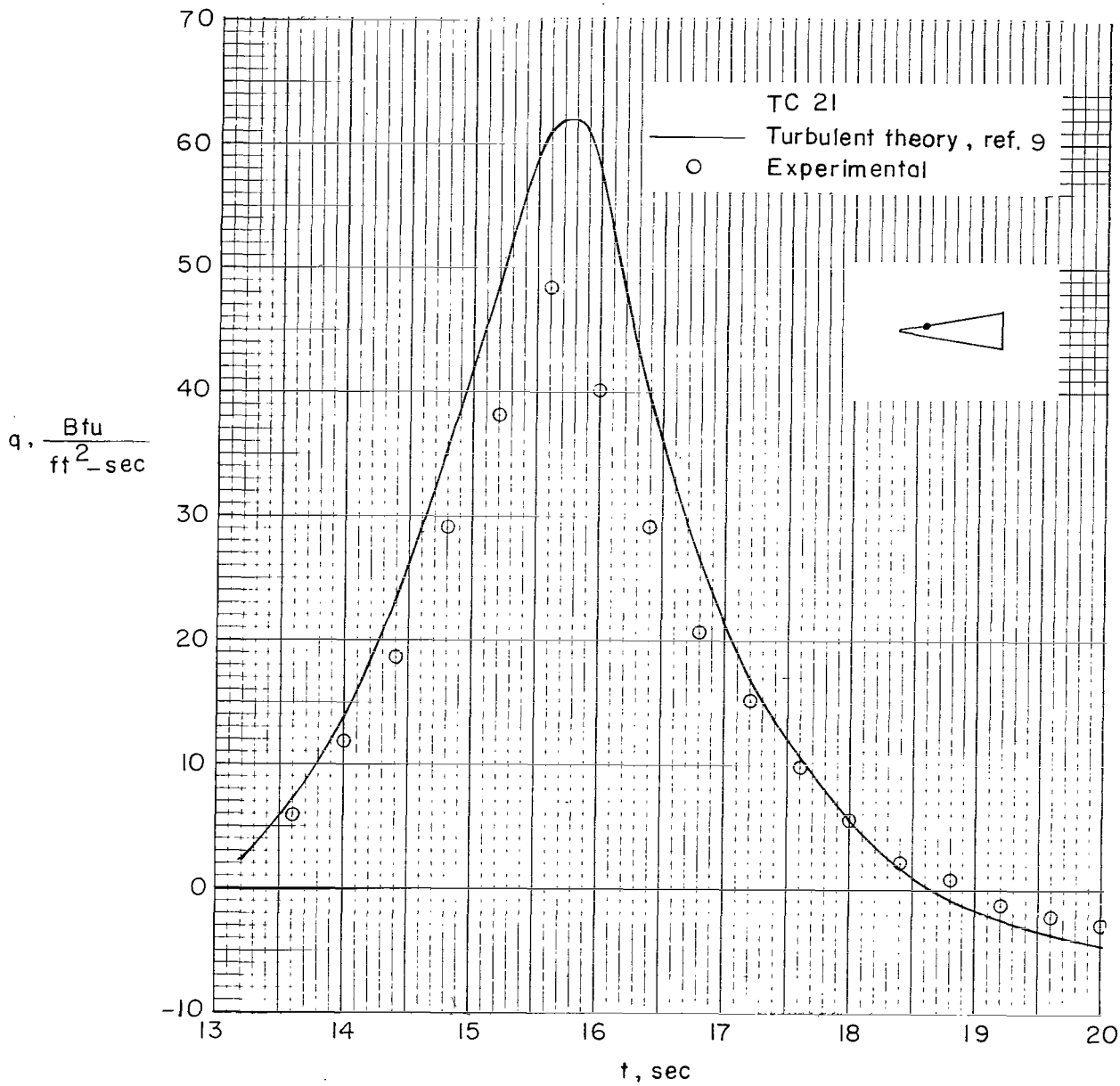

(b) Thermocouple 21.

Figure 17.- Continued.

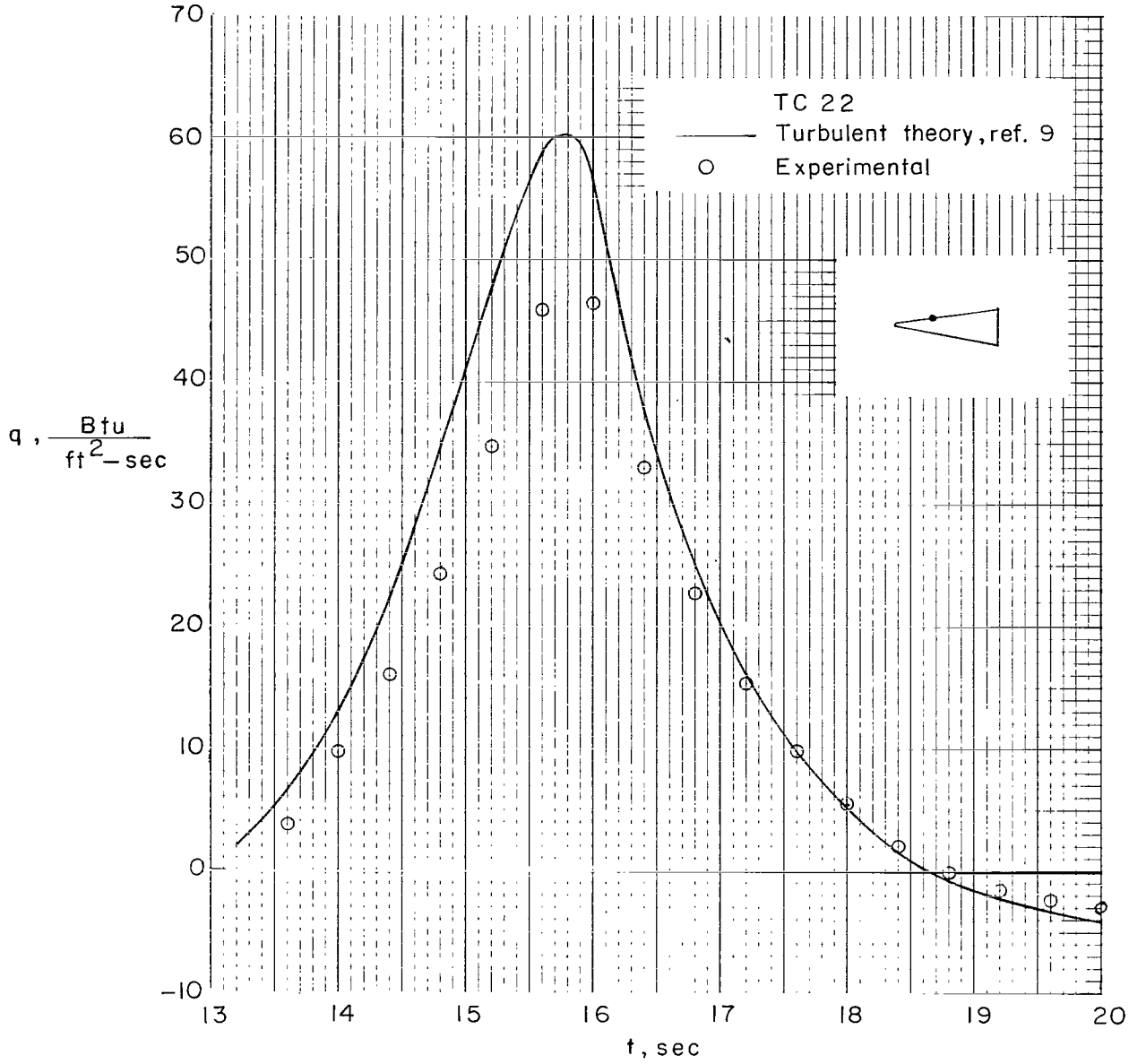

(c) Thermocouple 22.

Figure 17.- Continued.

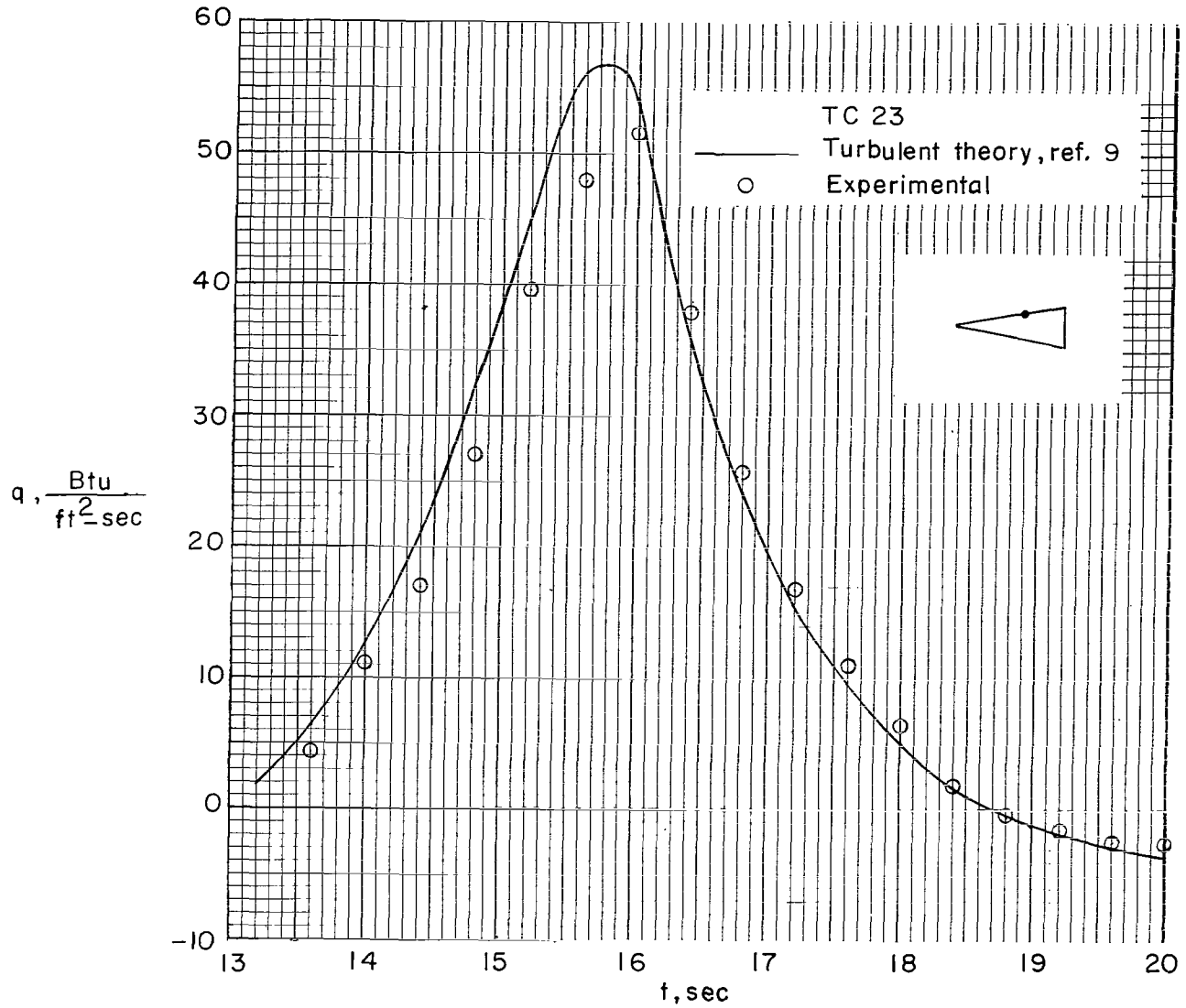

(d) Thermocouple 23.

Figure 17.- Continued.

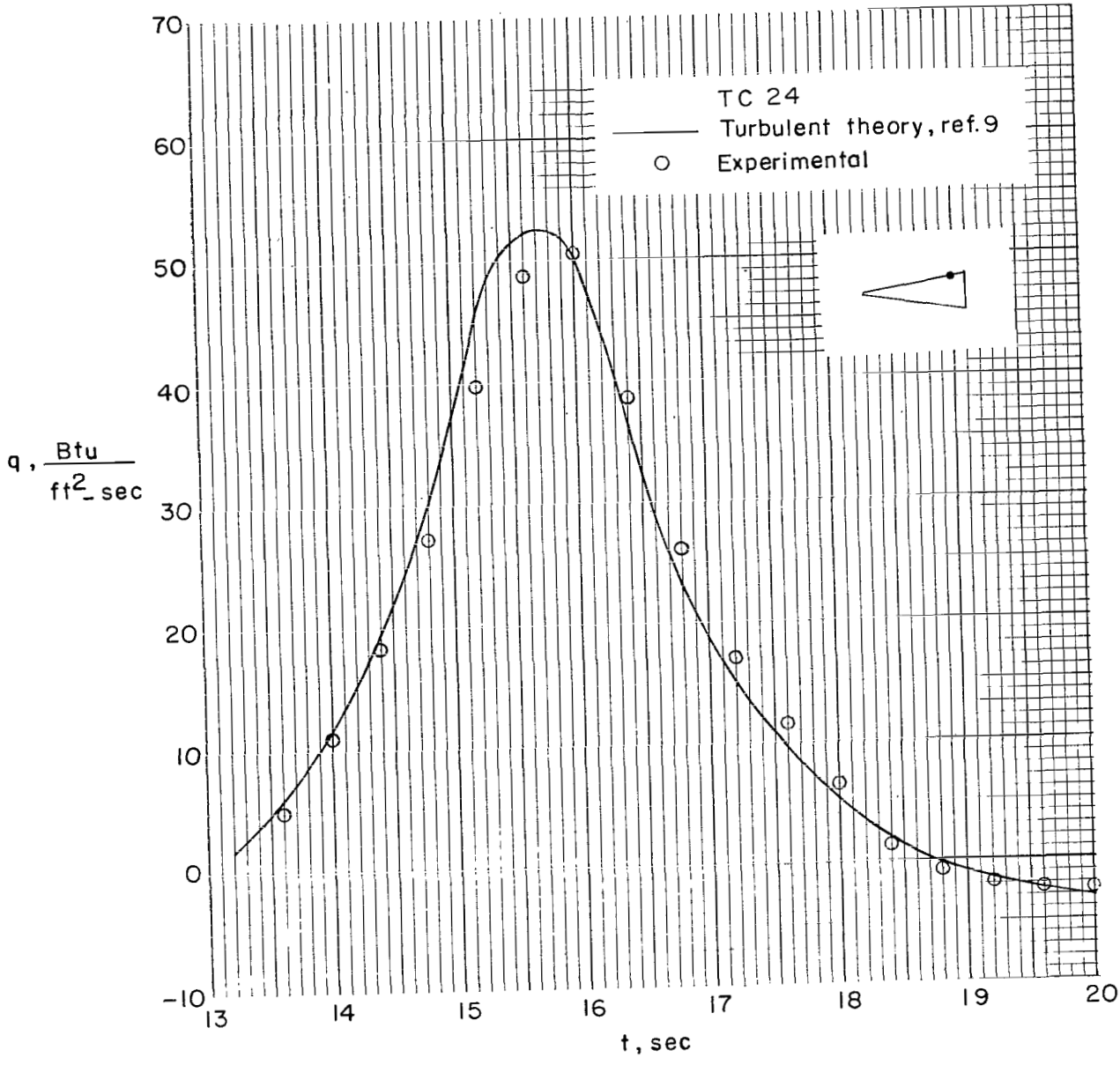

(e) Thermocouple 24.

Figure 17.- Concluded.

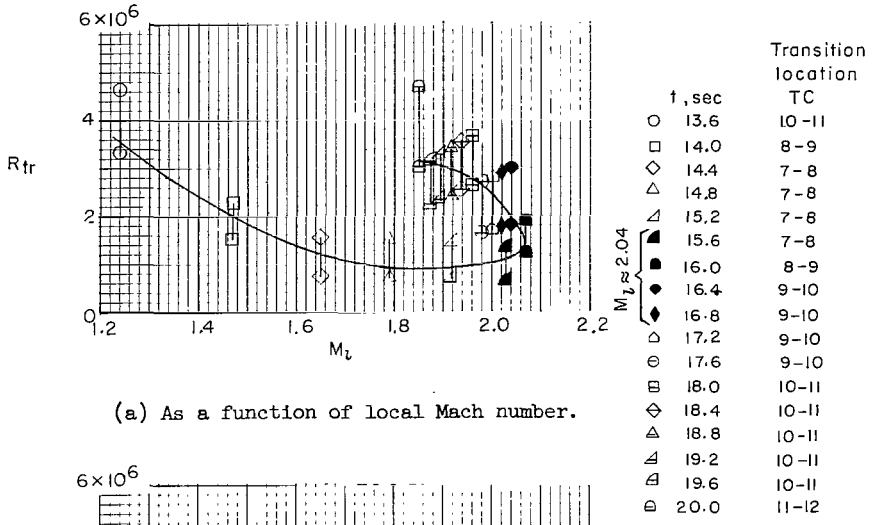

(a) As a function of local Mach number.

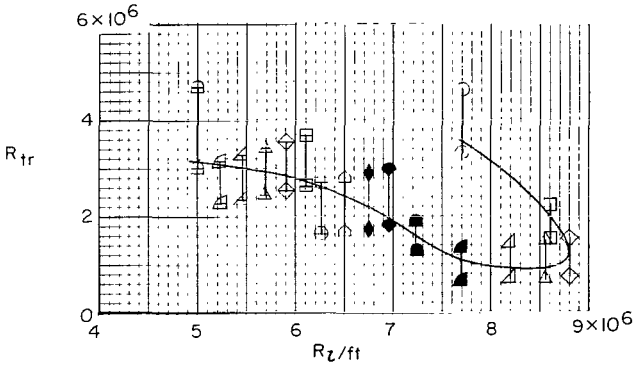

(b) As a function of local Reynolds number per foot.

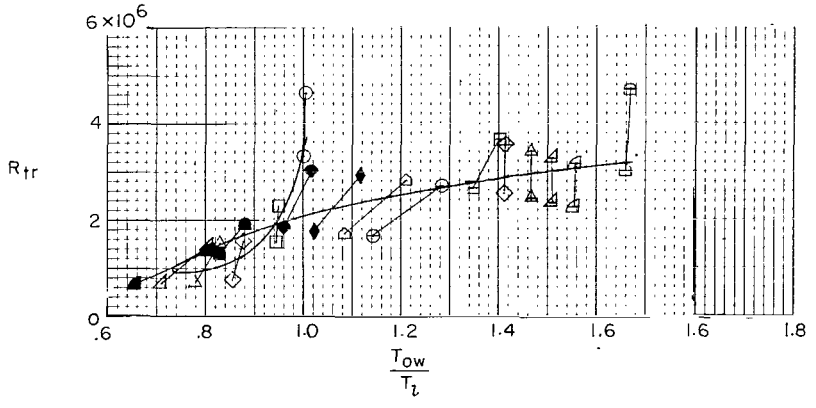

(c) As a function of $\frac{T_{ow}}{T_l}$.

Figure 18.- Transition Reynolds number.

"The aeronautical and space activities of the United States shall be conducted so as to contribute . . . to the expansion of human knowledge of phenomena in the atmosphere and space. The Administration shall provide for the widest practicable and appropriate dissemination of information concerning its activities and the results thereof."

—NATIONAL AERONAUTICS AND SPACE ACT OF 1958

NASA SCIENTIFIC AND TECHNICAL PUBLICATIONS

TECHNICAL REPORTS: Scientific and technical information considered important, complete, and a lasting contribution to existing knowledge.

TECHNICAL NOTES: Information less broad in scope but nevertheless of importance as a contribution to existing knowledge.

TECHNICAL MEMORANDUMS: Information receiving limited distribution because of preliminary data, security classification, or other reasons.

CONTRACTOR REPORTS: Technical information generated in connection with a NASA contract or grant and released under NASA auspices.

TECHNICAL TRANSLATIONS: Information published in a foreign language considered to merit NASA distribution in English.

TECHNICAL REPRINTS: Information derived from NASA activities and initially published in the form of journal articles.

SPECIAL PUBLICATIONS: Information derived from or of value to NASA activities but not necessarily reporting the results of individual NASA-programmed scientific efforts. Publications include conference proceedings, monographs, data compilations, handbooks, sourcebooks, and special bibliographies.

Details on the availability of these publications may be obtained from:

SCIENTIFIC AND TECHNICAL INFORMATION DIVISION

NATIONAL AERONAUTICS AND SPACE ADMINISTRATION

Washington, D.C. 20546